

Mica and feldspar as indicators of the evolution of a highly evolved granite-pegmatite system in the Tres Arroyos area (Central Iberian Zone, Spain)

I. Garate-Olave¹ · E. Roda-Robles¹ · P. P. Gil-Crespo¹ · A. Pesquera¹

Received: 22 December 2017 / Accepted: 4 July 2018 / Published online: 3 September 2018
© Springer Nature Switzerland AG 2018

Abstract

The aim of this study is to establish the petrogenetic links between the different granitic and aplopegmatitic units occurring in the Tres Arroyos granite-aplopegmatite system (Central Iberian Zone, Spain), from the textural and chemical variations in micas and feldspars. We aim to understand the differentiation mechanisms that allowed the extreme fractionation levels observed in the Li–F-richest dykes occurring in this aplopegmatite field. Major and trace elements in micas and feldspar from the different facies were analyzed by electron microprobe and LA-ICP-MS. Mica compositions define three different trends: muscovite-zinnwaldite-polylithionite, muscovite-trilithionite-polylithionite and biotite-zinnwaldite. The substitution mechanisms depend on the type of trend and on the stage of evolution. The K/Rb ratio and the Ba contents decrease in micas and K-feldspar with fractionation, whereas Li, Rb and Cs values increase. Lithium, Rb, Cs, Ba, Nb, and Ta show a clear tendency to get into the structure of the Fe-rich mica, whereas Be partitions preferably into the Al-micas. When Fe-micas are absent, Al-rich micas become the major sink for those trace elements. Phosphorus and Pb preferably get into the feldspars. In general, a linear and continuous variation of the K/Rb ratio with incompatible elements such as Cs, Rb or Li, and compatible such as Ba, both in micas and K-feldspar, supports a petrogenetic link between the Alburquerque batholith and the aplopegmatites via fractional crystallization.

Keywords Micas · Feldspars · Aplopegmatites · Granites · Tres Arroyos · Central Iberian Zone

Resumen

El propósito de este trabajo es establecer las relaciones petrogenéticas entre las distintas facies graníticas y aplopegmatíticas del sistema de Tres Arroyos (Zona Centro Ibérica, España) mediante las variaciones texturales y químicas en micas y feldespatos. También se intenta entender los diferentes mecanismos responsables del fraccionamiento extremo que se observa en los diques más ricos en Li-F. Se han analizado los elementos mayores y traza de las micas y de los feldespatos de las distintas facies por microsonda electrónica y ablación láser. Las micas pertenecen a tres tendencias composicionales: moscovita-zinnwaldita-polilitonita, moscovita-trilitonita-polilitonita y biotita-zinnwaldita. Los mecanismos de substitución varían según el tipo de mica y el grado de fraccionamiento. La razón K/Rb y los contenidos de Ba en micas y feldespato-K desciden con el fraccionamiento, mientras que los valores de Li, Rb y Cs aumentan. El Li, Rb, Ba, Nb y Ta se incorporan preferentemente en la estructura de las micas de Fe, mientras que el Be tiende a entrar en las de Al. En ausencia de micas de Fe, los elementos traza se incorporan principalmente en las micas de Al. El P y el Pb son los únicos elementos que se acumulan en los feldespatos. En general, la continua tendencia lineal que presentan las razones de K/Rb versus elementos incompatibles (Cs, Rb o Li), o elementos compatibles (Ba), tanto en micas como feldespato-K apoya la teoría de que las aplopegmatitas están genéticamente relacionadas con el granito de Alburquerque mediante un mecanismo de cristalización fraccionada.

Palabras clave Micas · Feldespatos · Aplopegmatitas · Granitos · Tres Arroyos · Zona Centro Ibérica

Electronic supplementary material The online version of this article (<https://doi.org/10.1007/s41513-018-0077-z>) contains supplementary material, which is available to authorized users.

Extended author information available on the last page of the article

1 Introduction

The Tres Arroyos aplopegmatite-granite system, located to the SW of the easternmost part of the Nisa-Alburquerque (NA) batholith (Badajoz, Spain), shows a complete fractionation sequence from monzogranite through barren to highly evolved aplopegmatic units (Gallego Garrido 1992; London et al. 1999; Garate-Olave et al. 2017). The gradual evolution is evidenced by the changes in the textures, mineralogy, and geochemistry of the different bodies, with a gradual enrichment in Li and other rare elements as the distance from the granite increases. Several studies show that the distribution of some elements (e.g., Li, Rb, Cs, Ti, Ge, Al...) in minerals such as feldspars, micas, tourmaline, or quartz is a good indicator of the fractionation degree in granite-pegmatite systems (e.g., Roda-Robles et al. 1993, 2012, 2015; Černý and Burt 1984; Foord et al. 1995; Roda et al. 2007a; Oyarzábal et al. 2009; Breiter et al. 2013; Marchal et al. 2014; Vieira et al. 2011; Drivenes et al. 2016; Müller et al. 2015; Garate-Olave et al. 2017; Pesquera et al. 2017). Micas and feldspars are common minerals in all the units of the Tres Arroyos granite-aplopegmatite system. Due to their capacity to host incompatible elements in the structure as well as their variable chemical composition, micas have frequently been used to obtain information about the crystallization conditions of pegmatites, their fractionation degree, and the petrogenetic relationships among granites and pegmatites (Černý and Burt 1984; Jolliff et al. 1992; Roda et al. 1999, 2007b; Oyarzábal et al. 2009; Vieira et al. 2011; Marchal et al. 2014). K-feldspar also has the capability to incorporate some specific trace elements, such as Li, Cs, or Rb, whose content usually increases with the degree of fractionation of these rocks (e.g., Černý et al. 1981; Oyarzábal et al. 2009; Wise and Brown 2010; Marchal et al. 2014, and many others).

The aim of this study is to establish the petrogenetic links between the different granitic and aplopegmatic units occurring in the granite-aplopegmatite system of Tres Arroyos from the textural and chemical variations in micas and K-feldspar. Likewise, we attempt to understand the differentiation mechanisms that allowed the extreme fractionation levels observed in the Li-F-richest dykes occurring in this aplopegmatite field.

2 Geological setting

The Tres Arroyos granite-aplopegmatite system is situated in the south of the Central-Iberian-Zone (CIZ) of the Variscan Massif, close to the limit with the Ossa Morena Zone.

The CIZ represents the westernmost part of the European Variscan Belt, which originated during the collision of the supercontinents Gondwana and Laurentia between 370 and 260 Ma ago (Martínez Catalán et al. 1996). This collision is related to the Variscan orogeny, where three major deformation events have been recognized (Martínez-Fernández 1974; Noronha et al. 1981). The CIZ is characterized by abundant granitic magmatism (Martínez et al. 1988). The Tres Arroyos area is located to the SW of the easternmost segment of one of these granitic bodies, known as the NA batholith (Fig. 1). This batholith intruded into a Precambrian metasedimentary sequence, including phyllites, slates, schists, quartzites, and metagreywackes, belonging to the metamorphic Schist-Greywacke Complex (SGC). Close to the NA batholith, slates, schists, and metagreywackes suffer contact metamorphism with a maximum width of up to 2 km (Santos-García and Casas-Ruiz 1978). The degree of metamorphism of these materials is low, with cordierite being the only contact metamorphic mineral developed together with a high-temperature biotite (González-Menéndez et al. 2010). The NA batholith may be classified as an S-type granite and is mainly composed of peraluminous monzogranite ($\approx 85\%$ of the outcrop), with minor two-mica leucogranitic facies (González Menéndez 1998; Solá et al. 1998). According to the Variscan deformation, this granite is considered to be late- to post-tectonic in relation to the D3 deformation event, with an emplacement age of 307–309 Ma (U–Pb SHRIMP data, Solá et al. 2009). The emplacement conditions were determined by comparing the mineral assemblage with the mineral stability fields, and it was concluded that the last level of emplacement might have been ≈ 2.5 kbar (González Menéndez et al. 2010).

3 Geology of the Tres Arroyos granite-aplopegmatite system

According to their chemistry, mineralogy, and textures, two granitic facies and three different types of aplopegmatite bodies (barren, intermediate, and Li-rich) have been distinguished in the Tres Arroyos system, all of them intruded into sediments of the SGC (Gallego Garrido 1992; Garate-Olave et al. 2017). These five units display a zonal distribution from the monzogranite up to the Li-richest aplopegmatites that occur furthest southwards from this granite (Fig. 1). The most important petrographic and mineralogical features of these units are as follows (Table 1):

- (1) The monzogranite shows a medium- to coarse-grained seriate to porphyritic texture (feldspar crystals < 9 cm long) (Fig. 2a). Quartz, K-feldspar, plagioclase, biotite, and muscovite are the main minerals, with apatite,

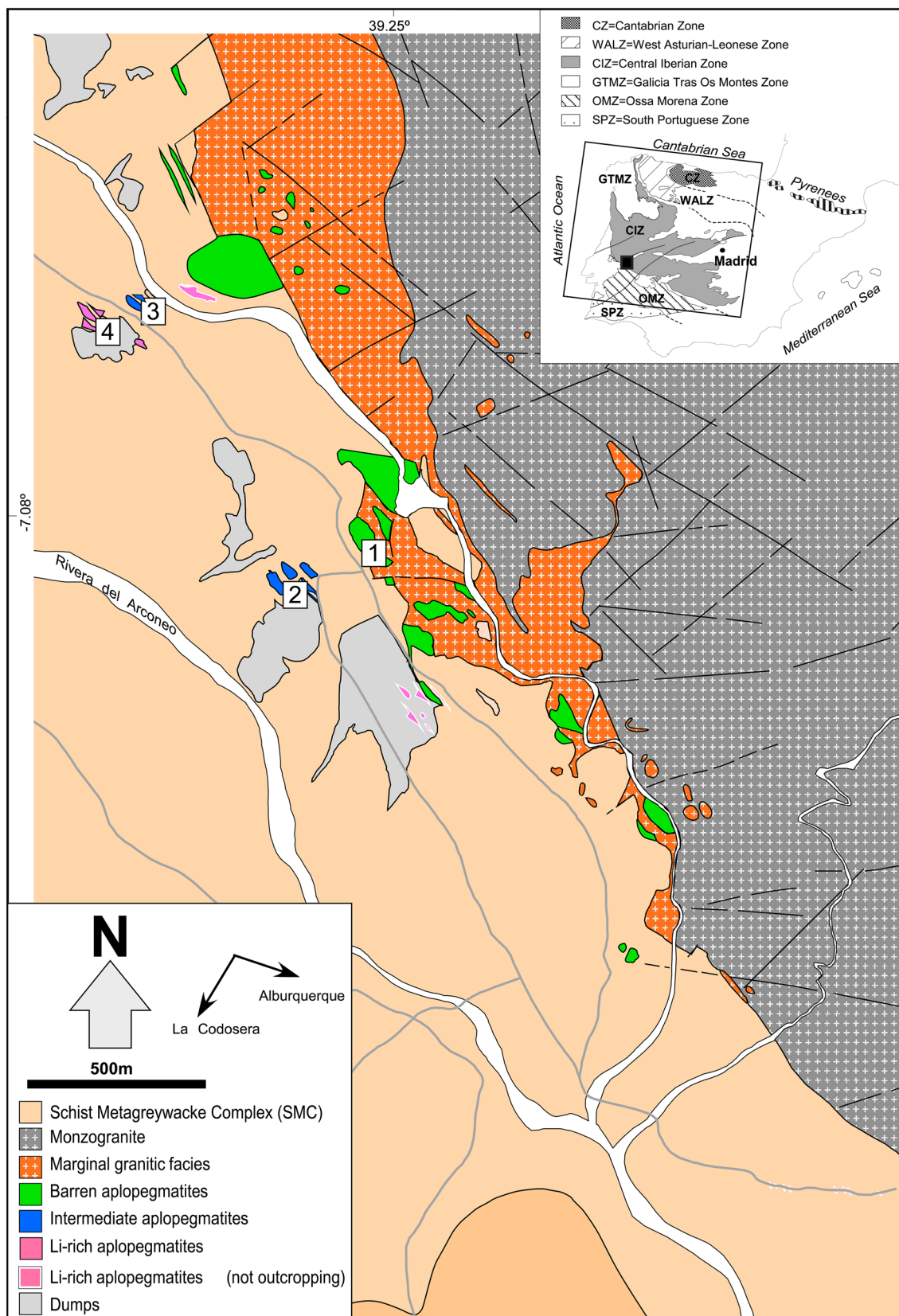


Fig. 1 Schematic geological map of the Central Iberian Zone (CIZ) and detailed map of the Tres Arroyos pegmatitic field (modified from Gallego-Garrido 1992 and published in Garate-Olave et al. 2017).

Locations of studied samples: (1) barren aplopegmatises; (2) intermediate aplopegmatises; (3) layered intermediate aplopegmatises; (4) Li-rich aplopegmatises

Table 1 Mineralogy and petrography of the different facies of the Tres Arroyos aplite-granite system

| Lithology | Mineralogy | Rock texture | Mica type | Mica texture and size | Feldspar type | Feldspar texture and size |
|--------------------------------|--|--|---|-----------------------------------|---|---|
| Porphyritic monzonitic granite | Quartz, K-feldspar, plagioclase, biotite, muscovite, cordierite, andalusite, tourmaline, zircon, apatite, monazite, oxides | Oriented porphyritic feldspar crystals | Biotite Muscovite | Fine to medium 0.1–1 cm | Subhedral to anhedral | K-feldspar (Or _{86.7–97.1}) Plagioclase (Ab _{75.6–96.4}) |
| Marginal granitic facies | Quartz, K-feldspar, plagioclase, tourmaline, biotite, muscovite, cordierite, andalusite, Fe–Li-muscovite, ilmenite | Biotite frequently concentrated in layers, Accessory tourmaline prisms | Biotite Muscovite Fe–Li-Muscovite | Very fine to fine 0.1–0.5 cm | Subhedral to anhedral | K-feldspar (Or _{80.6–95.9}) Plagioclase (Ab _{90.6–99.6}) |
| Barren aplite-granites | Quartz, plagioclase, K-feldspar, muscovite, tourmaline, zinnwaldite, topaz, Fe–Mn phosphates, apatite, Sn–Nb–Ta oxides | Chloritization and serization of the Al-silicates | Muscovite Fe–Li-Muscovite Zinnwaldite | Very fine to fine < 0.5 cm | Subhedral to anhedral | K-feldspar (Or _{55.2–89.2}) Plagioclase (Ab _{90.9–99.7}) |
| Intermediate aplite-granites | Quartz, plagioclase, K-feldspar, muscovite, topaz, Li–Al phosphates, Fe–Mn phosphates, apatite, Sn–Nb–Ta oxides | Feldspars display comb-texture | Muscovite Li-Muscovite Lepidolite | Very fine to fine < 0.1–0.5 cm | Subhedral to anhedral Interstitial In some cases fan-shaped | K-feldspar (Or _{91.1–97.7}) Plagioclase (Ab _{97.3–99.9}) |

Table 1 (continued)

| Lithology | Mineralogy | Rock texture | Mica type | Mica texture and size | Feldspar type | Feldspar texture and size |
|------------------------|--|--|---|-----------------------------------|--|---|
| Li-rich aplopegmatites | Quartz, plagioclase, K-feldspar, Li-Al-mica, topaz, Li-Al phosphates, Sn-Nb-Ta oxides, apatite | Rhythmic layering, some with a complex pattern, with alternating albite-rich and Li-mica rich layers | Muscovite Li-Muscovite Lepidolite | Very fine to fine < 0.1–0.6 cm | Subhedral to anhedral flakes Fan-shaped | K-feldspar (Or _{80.7–98.1}) Plagioclase (Ab _{97.4–99.8}) |

Very fine < 3 mm; fine = 3–6 mm; medium > 6 mm, coarse > 5 cm
Kfs K-feldspar, *Pf* plagioclase (Whitney and Evans 2010)

primary tourmaline, cordierite, andalusite, ilmenite, zircon, and monazite as minor or accessory phases (González Menéndez 1998) (Table 1). Andalusite and cordierite may be replaced by muscovite, chlorite, and/or tourmaline. Feldspar megacrystals show an orientated fabric across the whole of the batholith with a predominant E–WSW direction that is parallel to the maximum elongation of the batholith. In the studied area, close to the contact with the country-rock, the fabric shows N100–120E strike, dipping to the north (González Menéndez 1998).

- (2) In the Tres Arroyos area, the batholith exhibits a marginal facies with a variable extension (< 500 m) which is characterized by a finer grain size (up to 1 cm) and equigranular texture. The mineralogy is similar to that of the monzogranite, just with a noticeably higher abundance of tourmaline and certain enrichment in F, Li, and Fe in the muscovite.
- (3) The barren aplopegmatites outcrop near the NA batholith (the furthest one ≈ 300 m from the contact) (Fig. 1). These are irregular to tabular bodies with thicknesses from ≈ 1 m up to ≈ 5 m and a N135E strike, dipping slightly to the NE (Gallego Garrido 1992). Although locally it may be difficult to distinguish these aplopegmatites from the marginal granitic unit, up to 15 barren aplopegmatite bodies have been recognized in the field. The major mineralogical differences between the two lithologies are the lack of biotite and the occurrence of topaz and primary and secondary Fe–Mn phosphates in the aplopegmatites. Additionally, these dykes frequently display greenish coloured patches, most probably due to the meteoric alteration of some of the phosphates. These bodies do not show internal zoning. However, many of them are layered, with aplitic layers of variable thickness (from a few centimetres up to ≈ 60 cm) alternating with pegmatitic bands (Fig. 2b). The grain size changes from very fine grains (aplitic) up to 3-cm-long crystals. The biggest sizes usually correspond to feldspar comb-crystals that grow perpendicularly to the contacts and increase in width inward the dykes.
- (4) The intermediate bodies are subhorizontal leucocratic aplopegmatite dykes, discordant with the hosting metasediments and occurring a little further from the granite than the barren pegmatites (the furthest one ≈ 500 m from the contact) (Figs. 1, 2c). They are less abundant than the barren bodies, with only seven intermediate aplopegmatite dykes identified in the field. These bodies present variable thicknesses, from ≈ 1 m up to 8 m. Like the barren bodies, none of them show internal zoning, but some display a rhythmical layering, where albite-rich layers alternate with quartz-rich ones (Fig. 2d). Comb-crystals of feldspar (< 2 cm) are

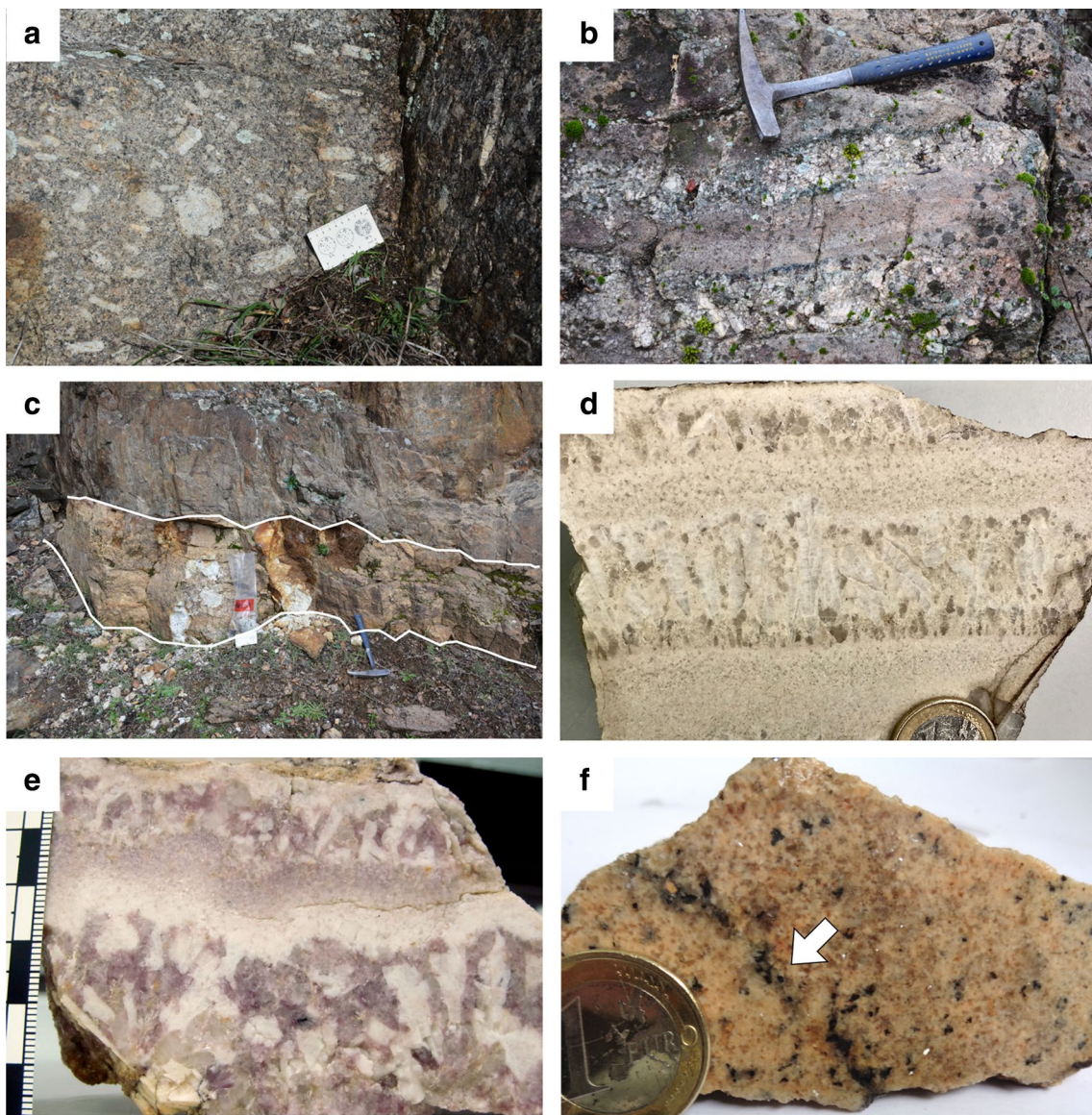


Fig. 2 **a** Porphyritic monzogranite with medium- to coarse-grained feldspar megacrysts; **b** barren layered aplopegmatite with alternating aplitic and pegmatitic layers; **c** subhorizontal intermediate aplopegmatitic dyke, discordant to host rock; **d** sample from an intermediate aplopegmatite, showing a simple layering pattern, with alternat-

ing albite-rich (albite showing comb-texture) and quartz-rich layers; **e** hand sample from a lepidolite-rich highly evolved aplopegmatitic dyke exhibiting a complex layering; **f** hand sample from the marginal granite showing a biotite-rich dark layer (white arrow)

common in the intermediate bodies as well. Their main mineral phases are albite and quartz, with K-feldspar and micas as minor constituents, and topaz, Li-Al-phosphates, Nb-Ta-Sn-oxides, and apatite as accessory phases. Despite the general homogeneity of these dykes, locally it is possible to observe Li-richer patches where fine-grained pinkish micas are abundant. This is interpreted as a result of the gradual transition from the intermediate to the most fractionated aplopegmatites, which are much richer in Li-micas. Similar to the Fregeneda-Almendra aplopegmatite field (Roda-Robles

et al. 2016), it is likely that these dykes show longitudinal zoning, with enrichment in Li southwards.

- (5) Highly evolved aplopegmatites constitute the third category. According to previous studies and the present work, in the Tres Arroyos area, around a dozen Li-F-rich aplopegmatites are described (the furthest one 1 km from the granite). Very abundant Li-rich micas, topaz, and amblygonite attest to the important enrichment in Li and F of these bodies. Like the barren and intermediate bodies, this type of aplopegmatites also shows no internal zoning, but often a layered internal

structure, with Li-mica-rich layers alternating with quartz + albite rich ones in the simplest case (Fig. 2e), whereas other, more complex layering patterns are less frequently observed.

The metasediments hosting the aplopegmatites show an important tourmalinization in the proximities of the bodies, in which biotite is replaced by tourmaline as a result of the activity of B-rich metasomatic fluids exsolved from the pegmatic melt (Fig. 3a).

4 Petrography

4.1 Micas

Micas associated with the different units of the granite-aplopegmatite system from the Tres Arroyos area belong to three different chemical trends, which include one or two mica series: (1) biotite-zinnwaldite, (2) muscovite-zinnwaldite-polylithionite, and (3) muscovite-trilithionite-polylithionite.

The biotite-zinnwaldite trend is restricted to the two granitic facies. Micas from the monzogranite show variable size (<1 cm), whereas in the marginal granitic unit micas are

usually smaller (<5 mm). In the two granitic units, the Fe-rich micas occur as subhedral, tabular crystals, frequently with metamictic halos produced by very fine zircon inclusions. These micas appear homogeneously distributed in the monzogranite. In contrast, they may appear concentrated in layers in the marginal granitic facies (Fig. 2f).

The micas from the muscovite-zinnwaldite-polylithionite trend are found in the monzogranite, marginal granite, and barren aplopegmatites. Primary muscovite associated with the monzogranite occurs as medium- to fine-grained, anhedral to subhedral crystals. Secondary muscovite is also present and is formed mainly by alteration of andalusite and/or cordierite. The Fe-bearing micas from this trend are mainly associated with the marginal granite and the barren aplopegmatites. They occur as medium- to fine-grained (<5 mm) crystals, exhibiting a slight pleochroism under the microscope, from light brown to colourless. Moreover, some fine zinnwaldite grains (<3 mm) from the barren aplopegmatites that are located in microfractures are considered secondary.

Micas from the muscovite-lepidolite (muscovite-trilithionite-polylithionite) series are mainly observed in the intermediate and Li-rich aplopegmatites. Muscovite and Li-muscovite are mainly related to the intermediate aplopegmatites. Their grain size is variable, from very fine up to 0.5 cm in length, occurring as flakes of silvery colours,

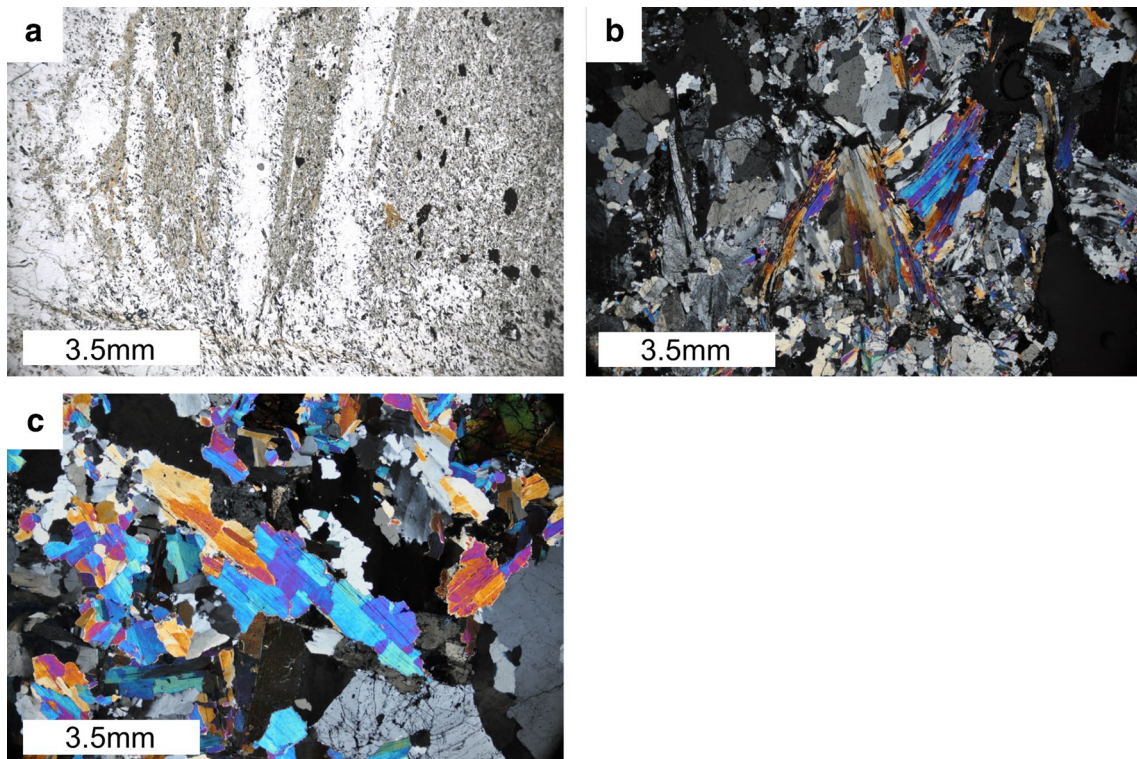


Fig. 3 Photomicrographs of: **a** tourmalinization of the host rock, where all the mass of fine-grained light brown crystals are tourmaline needles; **b** fan-shaped lepidolite crystals from the Li-rich dykes; **c** tabular-shaped lepidolite crystals

and occasionally growing interstitially among feldspar and quartz crystals. Lepidolite is the most common mica in the most fractionated aplopegmatite dykes. In these bodies, it is common to find eye-catching lilac-coloured micas in hand samples, with very fine (<0.1 cm) to fine (<0.6 cm) grain sizes. Under the microscope, lepidolite occurs as fan-shaped crystals (Fig. 3b) or as tabular flakes (Fig. 3c). Muscovite and Li-muscovite may also be observed locally in the Li-richest dykes, while some very fine-grained Li-muscovite crystals, almost saccharoid, occur in the intermediate aplopegmatites.

4.2 Feldspars

K-feldspar and plagioclase, which are present in the five units of the Tres Arroyos system, occur with different textures and modal proportions. In the granitic facies, K-feldspar and plagioclase are approximately equally abundant, whereas in the aplopegmatites, plagioclase clearly dominates over K-feldspar.

In the monzogranite, feldspars (microcline and albite-oligoclase) may appear as megacrystals (up to 9 cm), locally with a defined orientation (Fig. 2a). Microcline crystals display a characteristic cross-hatched twining (Fig. 4a) and, less frequently, the Carlsbad law. The development of abundant film to vein perthites is also common (Fig. 4a, b). Some of these veins underwent a subsolidus engrossment, giving as a result thicker lamellae often constituted by “chessboard” albite, which is usually attributed to Na-metasomatism processes (for more detail, see Smith 1974). Plagioclase is ubiquitous in the monzogranite, occurring either as individual crystals or as patches inside the crystals of K-Feldspar. The development of subgrains and deformation bands in plagioclase is appreciable in some grains.

K-feldspar is not as abundant in the aplopegmatite bodies as it is in the granitic facies. It appears as fine- to medium-sized (up to 2.5 cm) anhedral to subhedral crystals. In some cases, K-feldspar presents a “herringbone” texture as a result of the Manebach twinning and the perthitic lamellae located along the Murchison plane, with an angle of 158.5° between the two sets of lamellae (Fig. 4b). Comb-crystals of K-feldspar are frequent, increasing in width toward the core of the dykes. K-feldspar from the aplopegmatites also contains perthitic films, but the veins are scarcer than in the monzogranite. Apart from perthitic lamellae, some feldspar grains display poikilitic textures, where crystals may show locally oriented inclusions of other minerals, mainly plagioclase and quartz crystals, plus some small mica scales (Fig. 4c). More rarely, a “rapakivi”-like texture is also observed in the barren aplopegmatites, where fine-grained subhedral plagioclase crystals rim coarser K-feldspar crystals (Fig. 4d). Despite being quite common in other pegmatites, quartz-feldspar graphic intergrowths are not observed in any unit of

the Tres Arroyos system. Plagioclase is much more abundant than K-feldspar in the aplopegmatites, occurring mainly as fine- to medium-sized (<1 mm up to 7 mm) subhedral tabular crystals. In addition, in the layered dykes, plagioclase crystals grow as semi-radial aggregates (Fig. 4e) from a fine-grained quartz rich layer. Plagioclase comb-crystals, up to 2.5 cm in length, are also common. Plagioclase shows poly-synthetic twinning, including albite, ala, and pericline laws.

5 Data collection and analytical methods

The studied micas and feldspars were selected from the different facies of the NA granitic batholith and from the three aplopegmatite types distinguished in the Tres Arroyos field. To complete the sampling, a few of the studied specimens were collected from the dumps. Over 700 major-element microprobe analyses were obtained from polished thin sections using a JEOL Superprobe JXA-8900 M electron microprobe (EM) at the “Centro de Microscopía Electrónica Luis Bru” from the Universidad Complutense (Madrid, Spain) and a CAMECA SX100 at the research center of the University of Granada (Spain). For the first, the operating conditions were a voltage of 15 kV and beam current of 20nA. The calibrations standards used were sillimanite, albite, almandine, kaersutite, microcline, ilmenite, fluorapatite, scapolite, Ni alloy, chromite, gahnite, bentonite, and strontianite. The operating conditions used for the CAMECA SX100 were 15 kV and 15 nA for all elements. Data were reduced using the procedure of Pouchou and Pichoir (1985). Analytical errors are estimated to be of the order of $\pm 1\text{--}2\%$ for major elements and $\pm 10\%$ for minor elements. The structural formulae of micas and feldspar were calculated on the basis of 22 and 32 oxygens, respectively.

Trace elements, including Rb, Cs, Sn, Zn, Ba, Be, Nb, Ta, Zr, Ni, Tl, Pb, and REE for micas and Li, Be, Ni, Rb, Y, Zr, Nb, Sn, Cs, Ba, La, Ce, Pr, Nd, Sm, Eu, Gd, Tb, Dy, Ho, Er, Tm, Yb, Lu, Ta, Tl, and Pb for feldspar, were analysed by Laser-Ablation Inductively Coupled Plasma Mass Spectrometry (LA-ICP-MS) in SGIker at the Universidad del País Vasco (UPV/EHU). The LA-ICP-MS analyses were conducted with a 213-nm New Wave Research UP213 laser coupled to a Thermo Fisher Xseries-II ICP-MS with an Xt interface and a shielded plasma torch using the NIST SRM 612 glass for tuning. The ablation was carried out in a He atmosphere. The laser beam was fixed to an 80- μm -wide square section. The spot was pre-ablated for 45 s using a laser repetition rate of 10 Hz and 40% output energy. Then the spot was ablated for 60 s at 10 Hz with a laser output energy of 75%. A typical session of analysis of a single thin section began and ended with the analysis of the calibration standard NIST-612 glass, which was also analysed every ten spots to correct for drift. Silicon was used as the internal

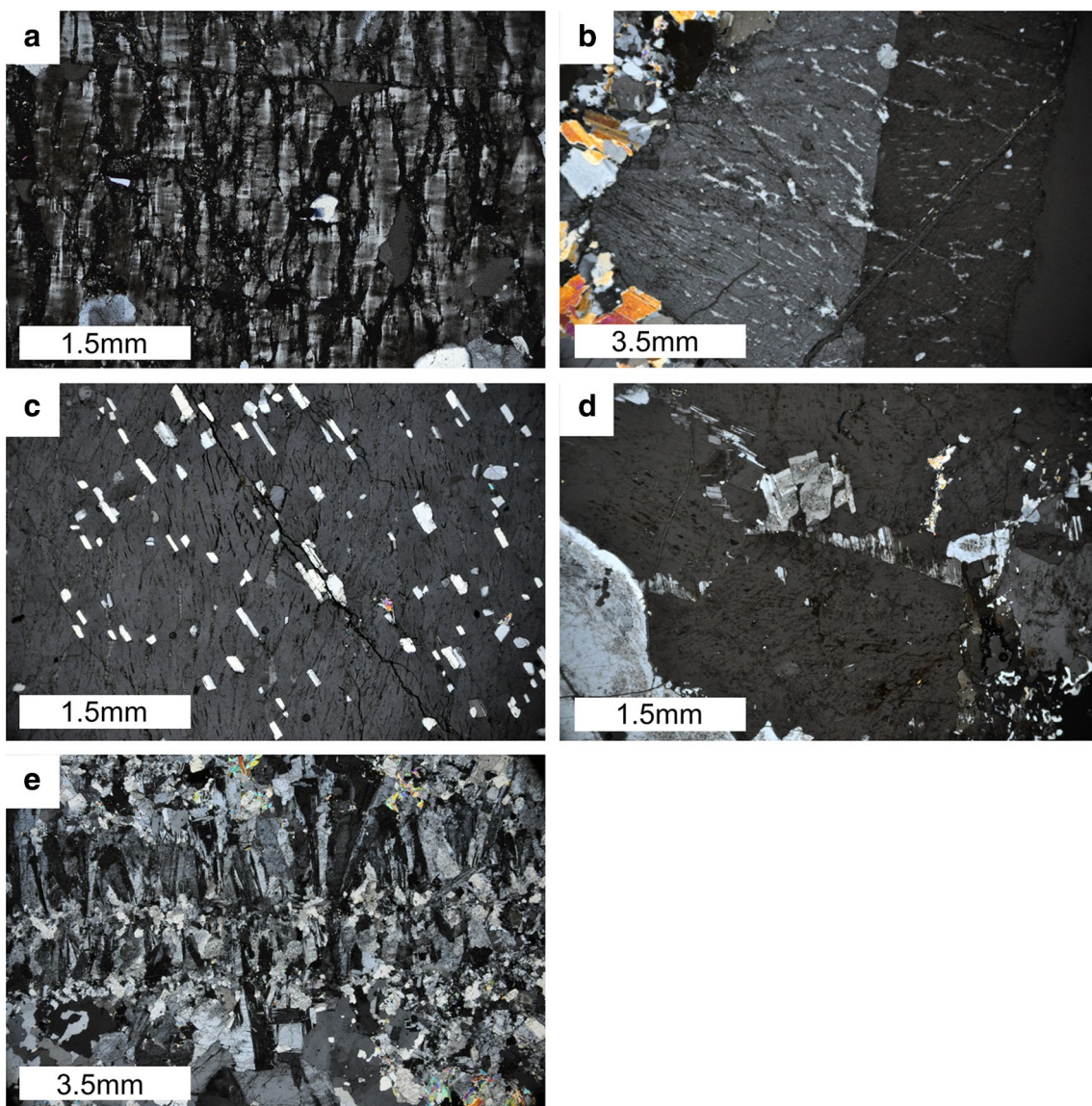


Fig. 4 Photomicrographs of: **a** cross-hatched twinned crystal of K-feldspar from the monzogranite, showing vein perthites (dark lines); **b** K-feldspar crystal from a Li-rich dyke, with the Manebach twin and perthitic lamellae located along the Murchison plane, with an angle of 158.5° between the two sets of lamellae; **c** poikilitic K-feldspar crystal from a barren aplopegmatite with inclusions of

quartz and plagioclase; **d** fine-grained subhedral plagioclase crystals rimming coarser K-feldspar crystals (“rapakivi”-like texture) from a barren aplopegmatite; **e** plagioclase crystals from a layered intermediate aplopegmatite, growing as semi-radial aggregates from a very fine-grained quartz layer

standard, and the accuracy and precision based on measurement of secondary standards (NIST-610) are provided in Supplementary Table 1. The limits of detection (LOD) were based on three times the standard deviation (3σ) of the measurements. LODs are also listed in Supplementary Table 1. Data reduction was carried out with Iolite 3 software (Paton et al. 2011). The Li_2O in micas was calculated according to the equation $\text{Li} = 03112 * \text{F}^{1.3414}$ (Roda-Robles et al. 2006).

Micas and feldspars were analysed on an X-ray diffractometer in SGIIker at the Universidad del País Vasco UPV/EHU using silicon as the internal standard. The equipment used was a PANalytical Xpert PRO with a copper tube ($\lambda_{\text{CuK}\alpha}$ media = 1.5418 Å, $\lambda_{\text{CuK}\alpha 1}$ = 1.54060 Å, and $\lambda_{\text{CuK}\alpha 2}$ = 1.54443 Å). The scanning conditions were 40 kV, 40 mA, and 5–70° 2Θ . Unit cell dimensions were obtained using a Unit Cell (Holland and Redfern 1997).

6 Results and discussion

6.1 Mineral Chemistry of micas

Micas from the three trends occurring in the Tres Arroyos area (muscovite-zinnwaldite-polylithionite, muscovite-trilithionite-polylithionite, and biotite-zinnwaldite) include Al-rich and/or Fe-rich micas (Table 2, Supplementary Tables 2, 3). In general, Al-rich micas show important chemical variations of some major and trace elements, mostly in relation to the different lithologies. Starting from the monzogranite, Al-rich micas follow the muscovite-zinnwaldite chemical trend, with a gradual enrichment in Fe–F–Li up to the barren aplopegmatites, parallel to a decrease in Al_2O_3 and SiO_2 (from 0.31 to 13.68 wt% for FeO , from 0 to 7.67 wt% for F, from 0 to 4.06 wt% for Li_2O , from 39.30 to 22.03 wt% for Al_2O_3 , and from 47.90 to 42.1 wt% for SiO_2) (Table 2, Supplementary Table 2, Fig. 5). Then, there is an inflection point and some micas from the barren aplopegmatites evolve toward the polylithionite term, becoming still richer in Li–F but poorer in Fe (from 13.68 to 9.87 wt% for FeO , from 7.67 to 8.76 wt% for F, and from 4.06 to 5.89 wt% for Li_2O) (Fig. 5).

In the case of the intermediate and the Li-rich aplopegmatites, the Al-rich micas evolve from dioctahedral muscovite towards trioctahedral lepidolite (trilithionite and polylithionite terms) (Fig. 5). The main variations are observed for Al_2O_3 , SiO_2 , F, and Li, which change broadly from averages of 35.05 wt% Al_2O_3 , 45.84 wt% SiO_2 , 2.07 wt% F, and 0.94 wt% Li_2O in the intermediate aplopegmatites to 26.43 wt% Al_2O_3 , 50.02 wt% SiO_2 , 8.05 wt% F, and 5.25 wt% Li_2O in the Li-rich bodies. Besides having the highest Li-contents, the micas from the Li-rich aplopegmatites are also characterized by very high contents of Rb_2O (1.05–4.22 wt%), corresponding to an intermediate member of the lepidolite-voloshinite series (Pekov et al. 2010), which is characteristic of highly fractionated pegmatitic environments (Černý et al. 2003, 2012). In contrast, the Cs contents remain quite low in all the analysed Li-rich micas, with the highest value being 0.77 wt% Cs_2O and most of the values being < 0.15 wt% Cs_2O . Micas from the Li-rich aplopegmatites are also the richest in MnO (0.19–0.63 wt%).

The series from dioctahedral muscovite to trioctahedral lepidolite is not continuous, with a compositional gap between 1.5 and 2.1 Li a.p.f.u. that corresponds to the “mixed forms” (Foster 1960; Hawthorne and Černý 1982). These mixed forms represent intermediate values between dioctahedral and trioctahedral micas and are inferred to be the result of submicroscopic interlayering of muscovite and lepidolite within the crystal. In the studied micas, the mixed forms are hardly represented (Fig. 5). As Marchal

et al. (2014) argued, microprobe analyses that plot in the muscovite-lepidolite compositional gap are the result of analysing areas containing interlayered Li-muscovite and lepidolite perpendicularly to the mica cleavage. With the sample arranged in that way, the microprobe beam would straddle both phases at the same time, and the results would hence correspond to a compositional average of the two interlayered micas.

The Fe-rich micas are only represented in the two granitic units (Fig. 5, Table 2, Supplementary Tables 2, 3). Starting from the Mg-richer siderophyllite associated with the monzogranite, there is a clear loss of Mg parallel to increases in Al, F, and Li in the siderophyllite from the marginal granite: from 18.46 to 20.06 wt% Al_2O_3 , 3.78–5.08 wt% MgO , 0–2.24 wt% F, and 0–0.92 wt% Li_2O in the monzogranite to 19.91–20.42 wt% Al_2O_3 , 0.05–1.16 wt% MgO , 2.42–2.81 wt% F, and 1.02–1.25 wt% Li_2O in the marginal granite.

The octahedral site occupancy for muscovite, which is in the range of 4.01–4.87, is close to or over the ideal of 4.0 a.p.f.u. The muscovite associated with the monzogranite shows the closest values to the ideal dioctahedral site occupancy, whereas the values are higher in the muscovites from the marginal granite (4.26–4.73), the barren aplopegmatites (4.13–4.85), and the intermediate bodies (4.07–4.87). These muscovites may be a mixed-layer form involving both dioctahedral and trioctahedral structures. The octahedral occupancy of the zinnwaldites from the barren aplopegmatites (5.02–6.69) and the lepidolites from the intermediate (5.72–6.12) and Li-rich aplopegmatites (5.576–6.031), in all the cases > 5 a.p.f.u., corresponds to trioctahedral structures. In contrast to the transition from muscovite to lepidolite, where a compositional gap is evidenced between the di- and trioctahedral structures (see above), the transition from dioctahedral muscovite to trioctahedral zinnwaldite is continuous, as stated by Monier and Robert (1986) (Fig. 5).

In addition to the important variations in the major element contents, the micas of the different units of the Tres Arroyos system also show significant differences in the trace element contents (Fig. 6a). Trace elements such as Rb, Cs, and Ta show a similar behaviour to Li, increasing from the monzogranite up to the most fractionated aplopegmatites. These elements show the lowest values in the micas from the monzogranite (860–1083 ppm Rb, 67–142 ppm Cs, and 2–4 ppm Ta for Al-micas and 631–3680 ppm Rb, 22–606 ppm Cs, and 3–26 ppm Ta for Fe-micas) and the highest contents in the micas from the Li-rich aplopegmatites (10400–30900 ppm Rb, 451–9000 ppm Cs, and 16–280 ppm Ta) (Fig. 6a). The opposite trend is shown by Ba, which, as expected, decreases dramatically with fractionation (130–237 and 0–20 ppm for Al-micas in the monzogranite and Li-rich aplopegmatites, respectively, and 48–982 for Fe-micas in the monzogranite) (Fig. 6a). Other elements such as Sn and Be exhibit more complex trends with a gradual increase

Table 2 Representative microprobe and LA-ICP-MS analyses of micas from the different facies of the Tres Arroyos aplopegmatite-granite system

| Lithology | Monzogranite | | | | | Marginal granitic facies | | | |
|---|--------------|---------|---------|--------|--------|--------------------------|---------|---------|---------|
| | Mineral | Bt | Bt | Ms | Ms | Ms | Bt | Bt | Ms |
| SiO ₂ | 34.700 | 34.684 | 46.430 | 45.406 | 45.406 | 33.977 | 34.488 | 46.107 | 45.324 |
| TiO ₂ | 2.884 | 3.860 | 0.044 | 0.274 | 0.274 | 1.878 | 2.628 | 0.183 | 0.186 |
| Al ₂ O ₃ | 18.462 | 18.514 | 36.413 | 36.049 | 36.049 | 20.419 | 19.910 | 33.047 | 34.332 |
| FeO | 24.640 | 24.556 | 0.999 | 1.243 | 1.243 | 27.480 | 27.036 | 2.812 | 2.692 |
| MnO | 0.278 | 0.200 | 0.063 | 0.016 | 0.016 | 0.206 | 0.196 | 0.069 | 0.025 |
| MgO | 4.868 | 3.780 | 0.296 | 0.579 | 0.579 | 0.855 | 1.164 | 0.220 | 0.160 |
| CaO | 0.008 | 0.000 | 0.022 | 0.002 | 0.002 | 0.006 | 0.000 | 0.000 | 0.027 |
| Na ₂ O | 0.108 | 0.117 | 0.862 | 0.901 | 0.901 | 0.157 | 0.192 | 0.881 | 0.792 |
| K ₂ O | 9.256 | 9.409 | 10.448 | 10.350 | 10.350 | 9.063 | 9.136 | 9.847 | 10.366 |
| SrO | n.a. | n.a. | n.a. | n.a. | n.a. | n.a. | n.a. | n.a. | n.a. |
| Rb ₂ O | 0.250 | 0.010 | 0.112 | n.a. | n.a. | 0.568 | 0.443 | 0.138 | 0.205 |
| Cs ₂ O | 0.020 | 0.010 | 0.000 | n.a. | n.a. | 0.023 | 0.012 | 0.001 | 0.000 |
| ZnO | n.a. | n.a. | n.a. | n.a. | n.a. | n.a. | n.a. | n.a. | 0.025 |
| Cr ₂ O ₃ | n.a. | n.a. | n.a. | n.a. | n.a. | n.a. | n.a. | n.a. | 0.000 |
| F | 1.233 | 1.969 | 0.424 | 0.516 | 0.516 | 2.511 | 2.530 | 2.872 | 2.492 |
| Li ₂ O* | 0.412 | 0.772 | 0.098 | 0.128 | 0.128 | 1.070 | 1.081 | 1.281 | 1.059 |
| H ₂ O** | 3.270 | 2.935 | 4.335 | 4.242 | 4.242 | 2.615 | 2.643 | 3.093 | 3.282 |
| Subtotal | 100.388 | 100.817 | 100.546 | 99.708 | 99.708 | 100.827 | 101.457 | 100.550 | 100.968 |
| O=F | 0.519 | 0.829 | 0.179 | 0.217 | 0.217 | 1.057 | 1.065 | 1.209 | 1.049 |
| Total | 99.869 | 99.987 | 100.368 | 99.490 | 99.490 | 99.770 | 100.392 | 99.341 | 99.918 |
| Structural formula on the basis of 22 O atoms | | | | | | | | | |
| Si | 5.399 | 5.377 | 6.139 | 6.069 | 6.069 | 5.355 | 5.382 | 6.208 | 6.089 |
| Al(IV) | 2.601 | 2.623 | 1.861 | 1.931 | 1.931 | 2.645 | 2.618 | 1.792 | 1.911 |
| (Z) | 8.000 | 8.000 | 8.000 | 8.000 | 8.000 | 8.000 | 8.000 | 8.000 | 8.000 |
| Al(VI) | 0.784 | 0.759 | 3.813 | 3.747 | 3.747 | 1.148 | 1.044 | 3.451 | 3.525 |
| Ti | 0.337 | 0.450 | 0.004 | 0.028 | 0.028 | 0.223 | 0.308 | 0.018 | 0.019 |
| Fe ²⁺ (t) | 3.206 | 3.183 | 0.110 | 0.139 | 0.139 | 3.622 | 3.528 | 0.317 | 0.302 |
| Mn | 0.037 | 0.026 | 0.007 | 0.002 | 0.002 | 0.028 | 0.026 | 0.008 | 0.003 |
| Mg | 1.129 | 0.874 | 0.058 | 0.115 | 0.115 | 0.201 | 0.271 | 0.044 | 0.032 |
| Li | 0.258 | 0.482 | 0.052 | 0.069 | 0.069 | 0.678 | 0.678 | 0.694 | 0.572 |
| Zn | 0.000 | 0.000 | 0.000 | 0.000 | 0.000 | 0.000 | 0.000 | 0.000 | 0.002 |
| (Y) | 5.751 | 5.774 | 4.046 | 4.100 | 4.100 | 5.899 | 5.856 | 4.532 | 4.456 |
| Vac(Y) | 0.249 | 0.226 | 1.954 | 1.900 | 1.900 | 0.101 | 0.144 | 1.468 | 1.544 |
| Ca | 0.001 | 0.000 | 0.003 | 0.000 | 0.000 | 0.001 | 0.000 | 0.000 | 0.004 |
| Na | 0.033 | 0.035 | 0.221 | 0.233 | 0.233 | 0.048 | 0.058 | 0.230 | 0.206 |
| K | 1.837 | 1.861 | 1.762 | 1.765 | 1.765 | 1.822 | 1.819 | 1.691 | 1.776 |
| Rb | 0.025 | 0.001 | 0.010 | 0.000 | 0.000 | 0.058 | 0.044 | 0.012 | 0.018 |
| Cs | 0.001 | 0.001 | 0.000 | 0.000 | 0.000 | 0.002 | 0.001 | 0.000 | 0.000 |
| (X) | 1.897 | 1.897 | 1.996 | 1.998 | 1.998 | 1.930 | 1.922 | 1.933 | 2.004 |
| F | 0.607 | 0.965 | 0.177 | 0.218 | 0.218 | 1.251 | 1.248 | 1.223 | 1.059 |
| OH | 3.393 | 3.035 | 3.823 | 3.782 | 3.782 | 2.749 | 2.752 | 2.777 | 2.941 |
| K/Rb | 73 | 1966 | 185 | — | — | 32 | 41 | 142 | 100 |
| K/Cs | 1391 | 2707 | — | — | — | 1169 | 2377 | 24549 | — |
| LA-ICP-MS analyses (ppm) | | | | | | | | | |
| Be | 4 | 3 | 10 | 6 | n.a. | 3 | 3 | 2 | n.a. |
| Ni | 27 | 21 | 1 | n.a. | n.a. | n.a. | n.a. | n.a. | n.a. |
| Rb | 2861 | 1104 | 879 | 860 | n.a. | 7207 | 6507 | 4790 | n.a. |

Table 2 (continued)

| Lithology | Monzogranite | | | | | Marginal granitic facies | | | |
|--------------------------------|--------------------------|-----------------------|---------|---------|---------|-----------------------------|---------|--------|---------|
| Mineral | Bt | Bt | Ms | Ms | Ms | Bt | Bt | Ms | Ms-Znw |
| Y | 7 | n.a. | n.a. | n.a. | n.a. | n.a. | n.a. | n.a. | n.a. |
| Zr | 12 | 2 | 1 | 1 | n.a. | 2 | 2 | 1 | n.a. |
| Nb | 169 | 266 | 20 | 16 | n.a. | 722 | 828 | 287 | n.a. |
| Sn | 71 | 120 | 103 | 86 | n.a. | 252 | 183 | 134 | n.a. |
| Cs | 92 | 38 | 67 | 67 | n.a. | 359 | 145 | 36 | n.a. |
| Ba | 48 | 514 | 106 | 130 | n.a. | 474 | 19 | 3 | n.a. |
| La | n.a. | 0.043 | — | — | n.a. | — | — | n.a. | n.a. |
| Ce | n.a. | 0.156 | 0.026 | n.a. | n.a. | 0.035 | n.a. | n.a. | n.a. |
| Pr | n.a. | n.a. | n.a. | n.a. | n.a. | n.a. | n.a. | n.a. | n.a. |
| Nd | n.a. | n.a. | n.a. | n.a. | n.a. | n.a. | n.a. | n.a. | n.a. |
| Sm | n.a. | n.a. | n.a. | n.a. | n.a. | n.a. | n.a. | n.a. | n.a. |
| Eu | n.a. | n.a. | n.a. | n.a. | n.a. | n.a. | n.a. | n.a. | n.a. |
| Gd | n.a. | n.a. | n.a. | n.a. | n.a. | n.a. | n.a. | n.a. | n.a. |
| Tb | n.a. | n.a. | n.a. | n.a. | n.a. | n.a. | n.a. | n.a. | n.a. |
| Dy | n.a. | n.a. | n.a. | n.a. | n.a. | n.a. | n.a. | n.a. | n.a. |
| Ho | n.a. | n.a. | n.a. | n.a. | n.a. | n.a. | n.a. | n.a. | n.a. |
| Er | n.a. | n.a. | n.a. | n.a. | n.a. | n.a. | n.a. | n.a. | n.a. |
| Tm | n.a. | n.a. | n.a. | n.a. | n.a. | n.a. | n.a. | n.a. | n.a. |
| Yb | n.a. | n.a. | n.a. | n.a. | n.a. | n.a. | n.a. | n.a. | n.a. |
| Lu | — | n.a. | n.a. | n.a. | n.a. | n.a. | n.a. | n.a. | n.a. |
| Ta | 25 | 15 | 4 | 4 | n.a. | 67 | 68 | 17 | n.a. |
| Tl | 13 | 10 | 3 | 3 | n.a. | 33 | 27 | 11 | n.a. |
| Pb | 5 | 4 | 3 | 2 | n.a. | — | — | — | n.a. |
| Lithology | Marginal granitic facies | Barren aplopegmatites | | | | Intermediate aplopegmatites | | | |
| Mineral | Ms-Znw | Ms-Znw | Ms-Znw | Znw | Znw | Ms | Ms | Ms | Ms |
| SiO ₂ | 45.180 | 45.630 | 44.511 | 43.409 | 42.350 | 46.081 | 45.537 | 46.669 | 46.600 |
| TiO ₂ | 0.128 | 0.150 | 0.265 | 0.000 | 0.305 | 0.092 | 0.004 | 0.146 | 0.113 |
| Al ₂ O ₃ | 34.356 | 29.751 | 30.300 | 22.710 | 26.848 | 35.671 | 37.341 | 34.961 | 34.997 |
| FeO | 2.853 | 5.795 | 5.959 | 10.965 | 10.682 | 1.023 | 0.878 | 1.497 | 1.496 |
| MnO | 0.077 | 0.076 | 0.125 | 0.241 | 0.120 | 0.063 | 0.045 | 0.042 | 0.017 |
| MgO | 0.259 | 0.047 | 0.061 | 0.118 | 0.140 | 0.013 | 0.018 | 0.074 | 0.032 |
| CaO | 0.000 | 0.014 | 0.030 | 0.000 | 0.037 | 0.000 | 0.000 | 0.016 | 0.009 |
| Na ₂ O | 0.889 | 0.484 | 0.156 | 0.150 | 0.286 | 0.431 | 0.600 | 0.543 | 0.765 |
| K ₂ O | 10.054 | 10.193 | 10.152 | 9.452 | 10.056 | 10.350 | 10.395 | 10.187 | 9.878 |
| SrO | n.a. | n.a. | n.a. | n.a. | n.a. | n.a. | n.a. | n.a. | n.a. |
| Rb ₂ O | 0.000 | 0.847 | 0.603 | 0.880 | 0.495 | 0.412 | 0.372 | 0.049 | 0.000 |
| Cs ₂ O | n.a. | 0.014 | 0.000 | 0.000 | 0.000 | 0.004 | 0.013 | 0.018 | 0.006 |
| ZnO | n.a. | n.a. | 0.187 | 0.156 | 0.237 | n.a. | n.a. | n.a. | n.a. |
| Cr ₂ O ₃ | n.a. | n.a. | 0.000 | 0.000 | 0.000 | n.a. | n.a. | n.a. | n.a. |
| F | 2.614 | 3.433 | 4.228 | 8.958 | 6.146 | 1.264 | 0.816 | 1.427 | 2.345 |
| Li ₂ O* | 1.129 | 1.628 | 2.152 | 5.893 | 3.555 | 0.426 | 0.237 | 0.501 | 0.976 |
| H ₂ O** | 3.223 | 2.723 | 2.343 | 0.000 | 1.341 | 3.879 | 4.130 | 3.817 | 3.402 |
| Subtotal | 100.764 | 100.785 | 101.072 | 102.932 | 102.598 | 99.709 | 100.385 | 99.946 | 100.636 |
| O=F | 1.100 | 1.445 | 1.780 | 3.772 | 2.588 | 0.532 | 0.344 | 0.601 | 0.987 |
| Total | 99.664 | 99.339 | 99.292 | 99.160 | 100.010 | 99.177 | 100.041 | 99.345 | 99.649 |

Table 2 (continued)

| Lithology | Marginal granitic facies | Barren aplopegmatites | | | | | Intermediate aplopegmatites | | | |
|---|--------------------------|-----------------------|--------|-------|-------|-------|-----------------------------|-------|-------|--|
| Mineral | Ms-Znw | Ms-Znw | Ms-Znw | Znw | Znw | Ms | Ms | Ms | Ms | |
| Structural formula on the basis of 22 O atoms | | | | | | | | | | |
| Si | 6.073 | 6.290 | 6.140 | 6.161 | 5.970 | 6.171 | 6.046 | 6.229 | 6.192 | |
| Al(IV) | 1.927 | 1.710 | 1.860 | 1.839 | 2.030 | 1.829 | 1.954 | 1.771 | 1.808 | |
| (Z) | 8.000 | 8.000 | 8.000 | 8.000 | 8.000 | 8.000 | 8.000 | 8.000 | 8.000 | |
| Al(VI) | 3.515 | 3.123 | 3.066 | 1.960 | 2.430 | 3.800 | 3.889 | 3.728 | 3.673 | |
| Ti | 0.013 | 0.016 | 0.027 | 0.000 | 0.032 | 0.009 | 0.000 | 0.015 | 0.011 | |
| Fe ²⁺ (t) | 0.321 | 0.668 | 0.687 | 1.301 | 1.259 | 0.115 | 0.097 | 0.167 | 0.166 | |
| Mn | 0.009 | 0.009 | 0.015 | 0.029 | 0.014 | 0.007 | 0.005 | 0.005 | 0.002 | |
| Mg | 0.052 | 0.010 | 0.013 | 0.025 | 0.029 | 0.003 | 0.003 | 0.015 | 0.006 | |
| Li | 0.610 | 0.902 | 1.194 | 3.364 | 2.015 | 0.229 | 0.127 | 0.269 | 0.522 | |
| Zn | 0.000 | 0.000 | 0.019 | 0.016 | 0.025 | 0.000 | 0.000 | 0.000 | 0.000 | |
| (Y) | 4.520 | 4.728 | 5.021 | 6.695 | 5.805 | 4.163 | 4.122 | 4.199 | 4.380 | |
| Vac(Y) | 1.480 | 1.272 | 0.979 | 0.000 | 0.195 | 1.837 | 1.878 | 1.801 | 1.620 | |
| Ca | 0.000 | 0.002 | 0.004 | 0.000 | 0.006 | 0.000 | 0.000 | 0.002 | 0.001 | |
| Na | 0.232 | 0.129 | 0.042 | 0.041 | 0.078 | 0.112 | 0.154 | 0.141 | 0.197 | |
| K | 1.724 | 1.792 | 1.786 | 1.711 | 1.808 | 1.768 | 1.761 | 1.734 | 1.674 | |
| Rb | 0.000 | 0.075 | 0.053 | 0.080 | 0.045 | 0.035 | 0.032 | 0.004 | 0.000 | |
| Cs | 0.000 | 0.001 | 0.000 | 0.000 | 0.000 | 0.000 | 0.001 | 0.001 | 0.000 | |
| (X) | 1.956 | 2.000 | 1.886 | 1.833 | 1.937 | 1.915 | 1.947 | 1.882 | 1.873 | |
| F | 1.111 | 1.496 | 1.844 | 4.020 | 2.739 | 0.535 | 0.343 | 0.602 | 0.985 | |
| OH | 2.889 | 2.504 | 2.156 | 0.000 | 1.261 | 3.465 | 3.657 | 3.398 | 3.015 | |
| K/Rb | — | 24 | 33 | 21 | 40 | 50 | 55 | 410 | — | |
| K/Cs | — | 2163 | — | — | — | 7741 | 2468 | 1731 | 4617 | |
| LA-ICP-MS analyses (ppm) | | | | | | | | | | |
| Be | 4 | 13 | n.a. | n.a. | n.a. | 39 | 81 | 28 | 27 | |
| Ni | n.a. | n.a. | n.a. | n.a. | n.a. | n.a. | n.a. | n.a. | n.a. | |
| Rb | 4540 | 7690 | n.a. | n.a. | 15000 | 4152 | 3790 | 1322 | 2308 | |
| Y | n.a. | n.a. | n.a. | n.a. | n.a. | n.a. | n.a. | n.a. | n.a. | |
| Zr | 2 | 1 | n.a. | n.a. | n.a. | 2 | n.a. | n.a. | n.a. | |
| Nb | 296 | 271 | n.a. | n.a. | 434 | 97 | 76 | 108 | 89 | |
| Sn | 110 | 234 | n.a. | n.a. | 427 | 570 | 670 | 843 | 524 | |
| Cs | 27 | 167 | n.a. | n.a. | 3350 | 140 | 119 | 178 | 124 | |
| Ba | 3 | 2 | n.a. | n.a. | 3 | 12 | 5 | 372 | 65 | |
| La | 0.069 | — | n.a. | n.a. | n.a. | n.a. | n.a. | n.a. | n.a. | |
| Ce | n.a. | n.a. | n.a. | n.a. | n.a. | n.a. | n.a. | n.a. | — | |
| Pr | n.a. | n.a. | n.a. | n.a. | n.a. | n.a. | n.a. | n.a. | — | |
| Nd | n.a. | n.a. | n.a. | n.a. | n.a. | n.a. | n.a. | n.a. | n.a. | |
| Sm | n.a. | n.a. | n.a. | n.a. | n.a. | n.a. | n.a. | n.a. | — | |
| Eu | n.a. | n.a. | n.a. | n.a. | n.a. | n.a. | n.a. | 0.047 | n.a. | |
| Gd | n.a. | n.a. | n.a. | n.a. | n.a. | n.a. | n.a. | n.a. | — | |
| Tb | n.a. | n.a. | n.a. | n.a. | n.a. | n.a. | n.a. | n.a. | — | |
| Dy | n.a. | n.a. | n.a. | n.a. | n.a. | n.a. | n.a. | n.a. | — | |
| Ho | n.a. | n.a. | n.a. | n.a. | n.a. | n.a. | n.a. | n.a. | — | |
| Er | n.a. | n.a. | n.a. | n.a. | n.a. | n.a. | n.a. | n.a. | — | |
| Tm | n.a. | n.a. | n.a. | n.a. | n.a. | n.a. | n.a. | n.a. | — | |
| Yb | n.a. | n.a. | n.a. | n.a. | n.a. | n.a. | n.a. | n.a. | — | |
| Lu | n.a. | n.a. | n.a. | n.a. | n.a. | n.a. | n.a. | n.a. | — | |
| Ta | 14 | 24 | n.a. | n.a. | 133 | 67 | 68 | 112 | 57 | |
| Tl | 10 | 20 | n.a. | n.a. | 42 | 16 | 14 | 7 | 8 | |
| Pb | — | — | n.a. | n.a. | — | 17 | 22 | 13 | n.a. | |

Table 2 (continued)

| Lithology | Intermediate aplopegmatites | | | | Lithium rich aplopegmatites | | | | |
|---|-----------------------------|---------|---------|---------|-----------------------------|---------|---------|---------|---------|
| Mineral | Ms | Ms | Mixed | Lp | Ms | Mixed | Lp | Lp | Lp |
| SiO ₂ | 45.578 | 45.407 | 46.907 | 49.236 | 45.464 | 47.340 | 51.517 | 48.839 | 49.256 |
| TiO ₂ | 0.018 | 0.000 | 0.061 | 0.042 | 0.000 | 0.056 | 0.040 | 0.032 | 0.050 |
| Al ₂ O ₃ | 35.460 | 36.663 | 30.833 | 24.839 | 37.069 | 32.491 | 25.196 | 28.119 | 24.381 |
| FeO | 1.442 | 1.020 | 1.361 | 2.304 | 0.384 | 0.491 | 0.078 | 0.078 | 2.107 |
| MnO | 0.121 | 0.000 | 0.298 | 0.526 | 0.077 | 0.000 | 0.217 | 0.334 | 0.621 |
| MgO | 0.003 | 0.000 | 0.002 | 0.000 | 0.004 | 0.000 | 0.288 | 0.000 | 0.003 |
| CaO | 0.000 | 0.000 | 0.004 | 0.001 | 0.015 | 0.002 | 0.000 | 0.000 | 0.024 |
| Na ₂ O | 0.796 | 0.522 | 0.330 | 0.219 | 0.471 | 0.247 | 0.387 | 0.194 | 0.325 |
| K ₂ O | 10.129 | 10.774 | 10.249 | 10.092 | 10.864 | 10.833 | 9.651 | 10.190 | 10.031 |
| SrO | n.a. | n.a. | n.a. | n.a. | n.a. | n.a. | n.a. | n.a. | n.a. |
| Rb ₂ O | 0.386 | 0.325 | 1.703 | 2.449 | 0.337 | n.a. | 2.721 | 2.978 | 2.819 |
| Cs ₂ O | n.a. | n.a. | 0.032 | 0.056 | 0.000 | n.a. | 0.083 | 0.078 | 0.090 |
| ZnO | n.a. | n.a. | 0.000 | 0.000 | n.a. | n.a. | n.a. | n.a. | n.a. |
| Cr ₂ O ₃ | n.a. | n.a. | 0.000 | 0.000 | n.a. | n.a. | n.a. | n.a. | n.a. |
| F | 2.228 | 1.414 | 4.802 | 7.999 | 0.886 | n.a. | 8.503 | 7.785 | 8.444 |
| Li ₂ O* | 0.911 | 0.495 | 2.553 | 5.062 | 0.265 | 2.370 | 5.495 | 4.882 | 5.444 |
| H ₂ O** | 3.424 | 3.826 | 2.149 | 0.636 | 4.075 | 2.332 | 0.515 | 0.814 | 0.429 |
| Subtotal | 100.497 | 100.447 | 101.283 | 103.459 | 99.910 | 100.703 | 104.693 | 104.325 | 104.023 |
| O=F | 0.938 | 0.595 | 2.022 | 3.368 | 0.373 | 1.912 | 3.580 | 3.278 | 3.555 |
| Total | 99.559 | 99.851 | 99.261 | 100.091 | 99.537 | 98.791 | 101.113 | 101.046 | 100.468 |
| Structural formula on the basis of 22 O atoms | | | | | | | | | |
| Si | 6.100 | 6.056 | 6.356 | 6.668 | 6.066 | 6.330 | 6.795 | 6.502 | 6.665 |
| Al(IV) | 1.900 | 1.944 | 1.644 | 1.332 | 1.934 | 1.670 | 1.205 | 1.498 | 1.335 |
| (Z) | 8.000 | 8.000 | 8.000 | 8.000 | 8.000 | 8.000 | 8.000 | 8.000 | 8.000 |
| Al(VI) | 3.694 | 3.818 | 3.280 | 2.633 | 3.894 | 3.450 | 2.712 | 2.913 | 2.553 |
| Ti | 0.002 | 0.000 | 0.006 | 0.004 | 0.000 | 0.006 | 0.004 | 0.003 | 0.005 |
| Fe ²⁺ (t) | 0.161 | 0.114 | 0.154 | 0.261 | 0.043 | 0.055 | 0.009 | 0.009 | 0.238 |
| Mn | 0.014 | 0.000 | 0.034 | 0.060 | 0.009 | 0.000 | 0.024 | 0.038 | 0.071 |
| Mg | 0.001 | 0.000 | 0.000 | 0.000 | 0.001 | 0.000 | 0.057 | 0.000 | 0.001 |
| Li | 0.491 | 0.266 | 1.391 | 2.757 | 0.142 | 1.274 | 2.915 | 2.614 | 2.962 |
| Zn | 0.000 | 0.000 | 0.000 | 0.000 | 0.000 | 0.000 | 0.000 | 0.000 | 0.000 |
| (Y) | 4.362 | 4.198 | 4.866 | 5.715 | 4.089 | 4.785 | 5.721 | 5.576 | 5.830 |
| Vac(Y) | 1.638 | 1.802 | 1.134 | 0.285 | 1.911 | 1.215 | 0.279 | 0.424 | 0.170 |
| Ca | 0.000 | 0.000 | 0.001 | 0.000 | 0.002 | 0.000 | 0.000 | 0.000 | 0.004 |
| Na | 0.207 | 0.135 | 0.087 | 0.057 | 0.122 | 0.064 | 0.099 | 0.050 | 0.085 |
| K | 1.729 | 1.833 | 1.772 | 1.744 | 1.849 | 1.848 | 1.624 | 1.730 | 1.731 |
| Rb | 0.033 | 0.028 | 0.148 | 0.213 | 0.029 | 0.000 | 0.231 | 0.255 | 0.245 |
| Cs | 0.000 | 0.000 | 0.002 | 0.003 | 0.000 | 0.000 | 0.005 | 0.004 | 0.005 |
| (X) | 1.969 | 1.996 | 2.009 | 2.017 | 2.002 | 1.912 | 1.958 | 2.040 | 2.071 |
| F | 0.943 | 0.596 | 2.057 | 3.425 | 0.374 | 1.920 | 3.547 | 3.277 | 3.613 |
| OH | 3.057 | 3.404 | 1.943 | 0.575 | 3.626 | 2.080 | 0.453 | 0.723 | 0.387 |
| K/Rb | 52 | 66 | 12 | 8 | 64 | — | 7 | 7 | 7 |
| K/Cs | — | — | 964 | 538 | — | — | 347 | 389 | 333 |
| LA-ICP-MS analyses (ppm) | | | | | | | | | |
| Be | n.a. | n.a. | n.a. | n.a. | n.a. | n.a. | n.a. | 56 | 51 |
| Ni | n.a. | n.a. | n.a. | n.a. | n.a. | n.a. | n.a. | n.a. | n.a. |
| Rb | n.a. | n.a. | n.a. | n.a. | n.a. | n.a. | n.a. | 27100 | 25720 |
| Y | n.a. | n.a. | n.a. | n.a. | n.a. | n.a. | n.a. | n.a. | n.a. |

Table 2 (continued)

| Lithology | Intermediate aplopegmatites | | | | Lithium rich aplopegmatites | | | | |
|-----------|-----------------------------|------|-------|------|-----------------------------|-------|------|-------|-------|
| Mineral | Ms | Ms | Mixed | Lp | Ms | Mixed | Lp | Lp | Lp |
| Zr | n.a. | n.a. | n.a. | n.a. | n.a. | n.a. | n.a. | 0.434 | 0.543 |
| Nb | n.a. | n.a. | n.a. | n.a. | n.a. | n.a. | n.a. | 223 | 196 |
| Sn | n.a. | n.a. | n.a. | n.a. | n.a. | n.a. | n.a. | 409 | 360 |
| Cs | n.a. | n.a. | n.a. | n.a. | n.a. | n.a. | n.a. | 1280 | 1432 |
| Ba | n.a. | n.a. | n.a. | n.a. | n.a. | n.a. | n.a. | n.a. | n.a. |
| La | n.a. | n.a. | n.a. | n.a. | n.a. | n.a. | n.a. | n.a. | n.a. |
| Ce | n.a. | n.a. | n.a. | n.a. | n.a. | n.a. | n.a. | n.a. | n.a. |
| Pr | n.a. | n.a. | n.a. | n.a. | n.a. | n.a. | n.a. | n.a. | n.a. |
| Nd | n.a. | n.a. | n.a. | n.a. | n.a. | n.a. | n.a. | n.a. | n.a. |
| Sm | n.a. | n.a. | n.a. | n.a. | n.a. | n.a. | n.a. | n.a. | n.a. |
| Eu | n.a. | n.a. | n.a. | n.a. | n.a. | n.a. | n.a. | n.a. | n.a. |
| Gd | n.a. | n.a. | n.a. | n.a. | n.a. | n.a. | n.a. | n.a. | n.a. |
| Tb | n.a. | n.a. | n.a. | n.a. | n.a. | n.a. | n.a. | n.a. | n.a. |
| Dy | n.a. | n.a. | n.a. | n.a. | n.a. | n.a. | n.a. | n.a. | n.a. |
| Ho | n.a. | n.a. | n.a. | n.a. | n.a. | n.a. | n.a. | n.a. | n.a. |
| Er | n.a. | n.a. | n.a. | n.a. | n.a. | n.a. | n.a. | n.a. | n.a. |
| Tm | n.a. | n.a. | n.a. | n.a. | n.a. | n.a. | n.a. | n.a. | n.a. |
| Yb | n.a. | n.a. | n.a. | n.a. | n.a. | n.a. | n.a. | n.a. | n.a. |
| Lu | n.a. | n.a. | n.a. | n.a. | n.a. | n.a. | n.a. | n.a. | n.a. |
| Ta | n.a. | n.a. | n.a. | n.a. | n.a. | n.a. | n.a. | 113 | 74 |
| Tl | n.a. | n.a. | n.a. | n.a. | n.a. | n.a. | n.a. | 64 | 62 |
| Pb | n.a. | n.a. | n.a. | n.a. | n.a. | n.a. | n.a. | — | — |

*For more detail on calculations of the Li content see the text (“Data collection and analytical methods”)

**Calculated by stoichiometry (oxides given in wt%; cations in a.p.f.u., and trace elements in ppm)

from the monzogranite up to the intermediate pegmatites and then a slight decrease in the lepidolites from the Li-rich aplopegmatites (Sn values vary in the ranges of 86–161 and

66–131 ppm for Al-micas and Fe-micas, respectively in the monzogranite, 272–949 ppm for Al-micas in intermediate bodies, and 403–110 ppm for Al-micas in the most evolved dykes; Be values are in the ranges of 5–10 and 3–9 ppm for Al-micas and Fe-micas respectively in the monzogranite, 16–232 ppm for Al-micas in intermediate bodies, and 63–17 ppm for Al-micas in the most evolved dykes). Niobium increases from the monzogranite to the marginal granite (16–32 ppm for Al-micas and 19–296 ppm for Fe-micas; 74–1003 ppm for Al-micas and 103–849 ppm for Fe-micas, respectively), with intermediate values in the three aplopegmatite types (55–271 and 90–452 ppm for Al-micas and Fe–F-micas, respectively for the barren aplopegmatites; 62–114 and 85–428 ppm for Al-micas in intermediate and Li-rich aplopegmatites, respectively).

6.2 Substitution mechanisms in micas

Mica composition from the less fractionated units seems to be controlled by the muscovite-zinnwaldite exchange vector ($\text{Fe}^{2+}\text{LiAl}_{-1}^{\text{IV}}\text{Vac}_{-1}$) (Fig. 7a, b), becoming richer in Li–F–Fe from the monzogranite to the marginal granite. This suggests an important Fe activity in the less evolved melts, where

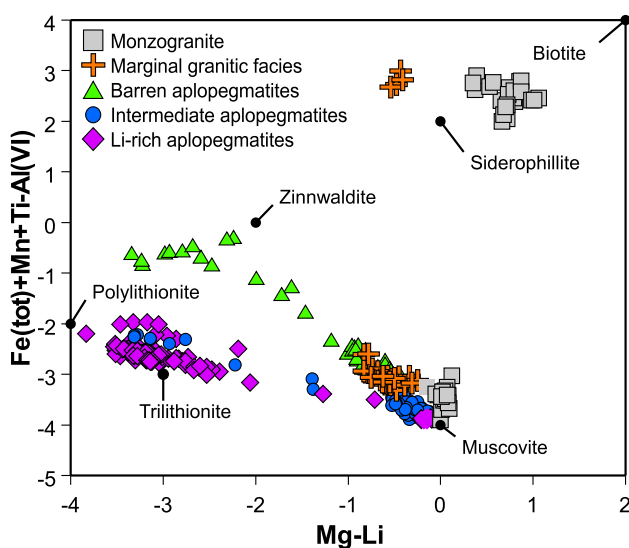


Fig. 5 Variation of (Mg–Li) vs. ($\text{Fe}_{\text{tot}} + \text{Mn} + \text{Ti} + \text{Al}^{\text{VI}}$) for the analysed micas (all data in a.p.f.u.)

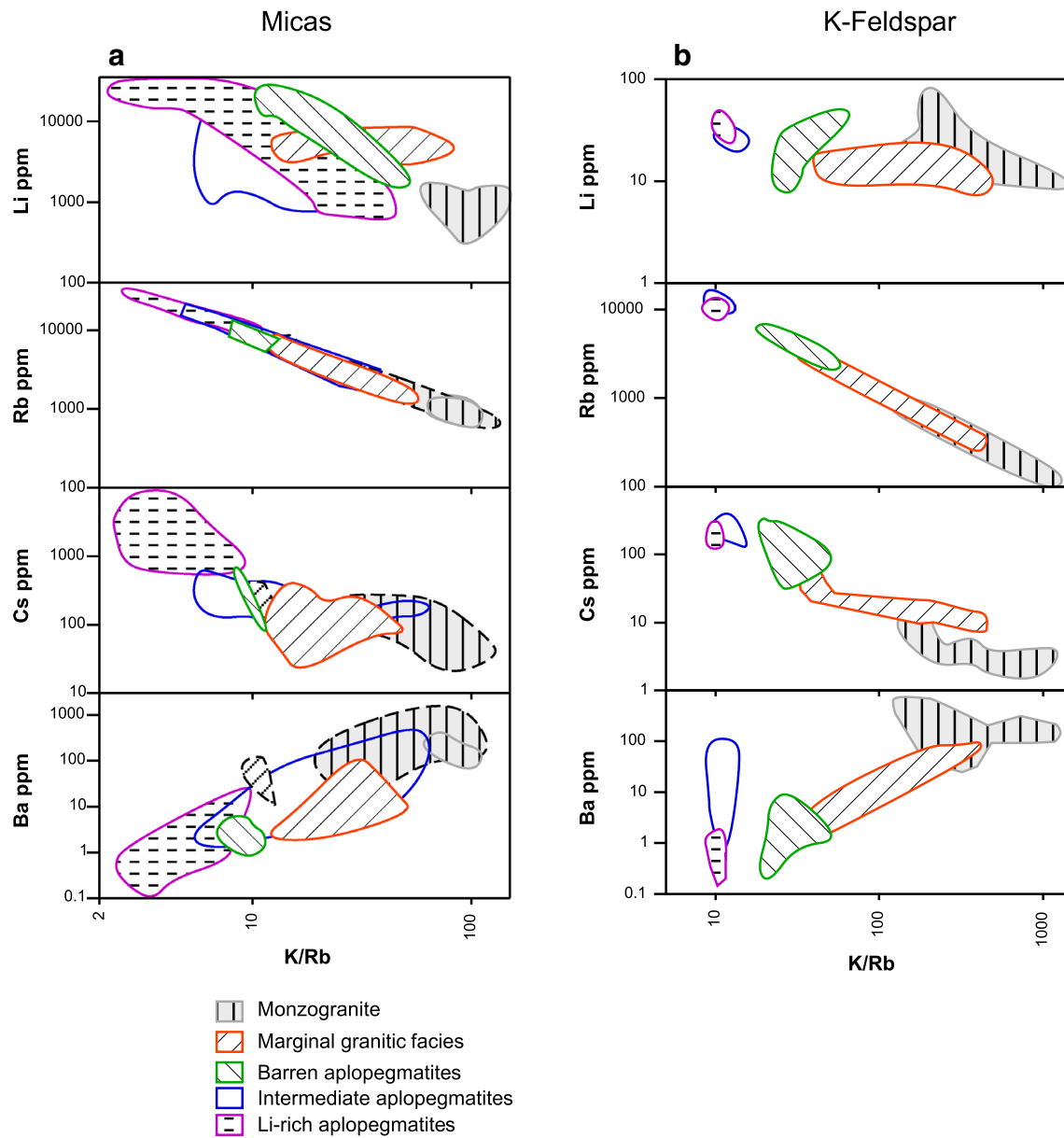


Fig. 6 Plot of the K/Rb ratio vs. Li, Rb, Cs, and Ba contents in **a** micas and **b** K-feldspar from the different facies distinguished in Tres Arroyos (continuous lines correspond to Al-micas and discontinuous lines correspond to Fe-micas) (all data in ppm)

other Fe-bearing minerals, such as schorl and Fe–Mn-phosphates, are also present. In the last stages of crystallization of the barren aplopegmatites the influence of this substitution mechanism decreases, and Al-micas evolve following the zinnwaldite-polylithionite exchange vector ($\text{SiLiAl}_{-1}^{\text{IV}}\text{Fe}_{-1}^{2+}$) (Fig. 7a, b). The Al-rich micas from the intermediate and Li-rich aplopegmatites reflect the extremely low Fe-contents in the very last residual melts, with the mica composition evolving from Li-poor terms (muscovite, mainly associated with the intermediate aplopegmatites) to the Li-rich end members (trilithionite and polylithionite, mainly associated with the Li-rich aplopegmatites). Most of the micas from the

intermediate aplopegmatites evolve through the substitution muscovite-polylithionite ($\text{Li}_2\text{SiAl}_{-1}^{\text{IV}}\text{Al}_{-1}^{\text{VI}}\text{Vac}_{-1}$) (Fig. 7c, d). Only the Li-richest micas in these intermediate bodies, as well as the Li-poorest ones from the Li-rich aplopegmatites, change their composition following the muscovite-trilithionite exchange vector ($\text{Li}_3\text{Al}_{-1}^{\text{VI}}\text{Vac}_{-2}$) (Fig. 7c, d). Finally, the chemical composition of the Li-richest micas from the Li-rich bodies evolves according to the trilithionite-polylithionite substitution mechanism ($\text{Si}_2\text{LiAl}_{-1}^{\text{IV}}\text{Al}_{-2}^{\text{VI}}$) (Fig. 7c, d).

The Fe-rich micas show a much shorter compositional trend, with the transition from Mg-rich siderophyllite in the monzogranite to siderophyllite in the marginal granite. The

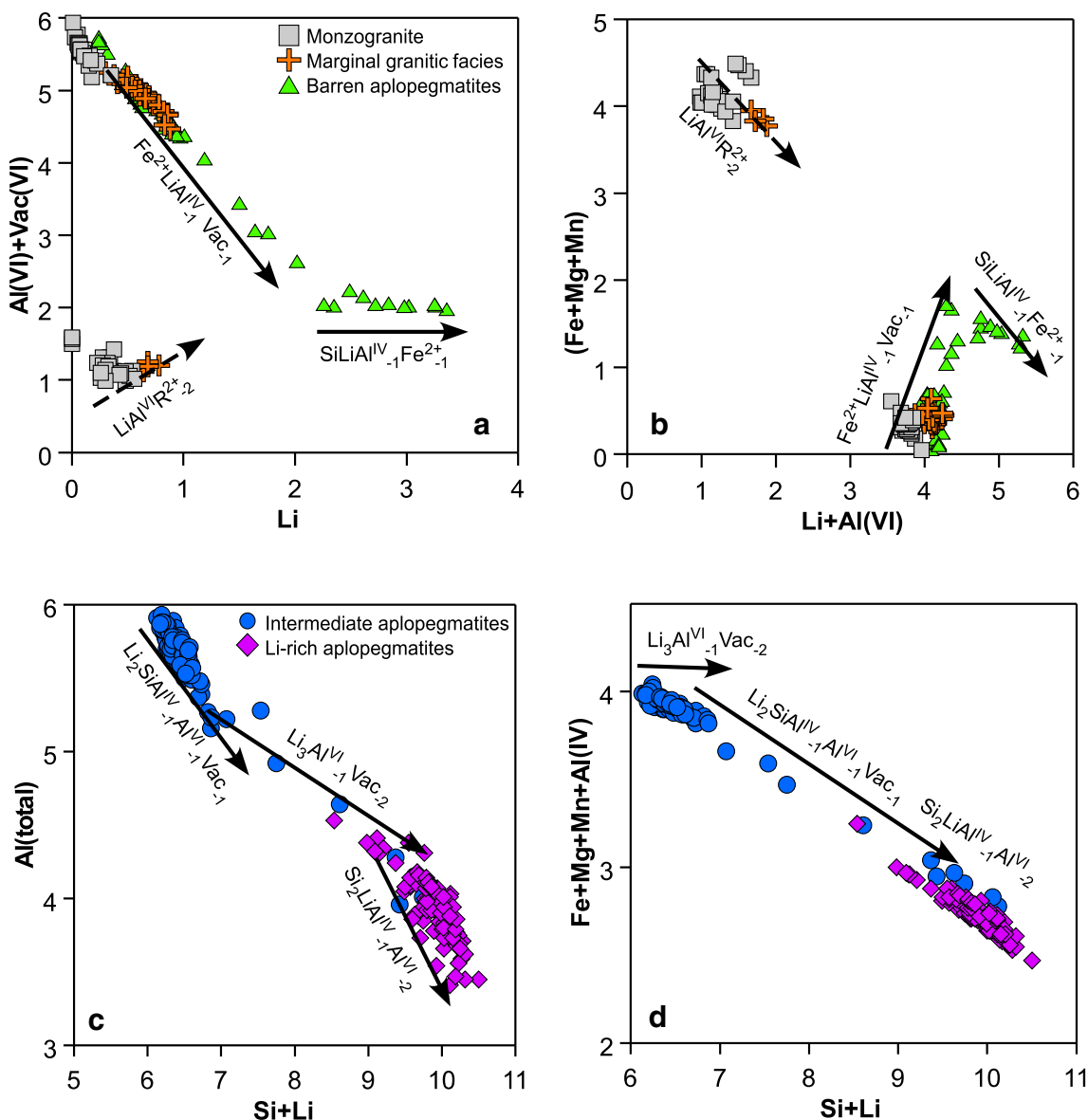


Fig. 7 Plots of **a** Li vs. $\text{Al}(\text{VI}) + \text{Vac}(\text{VI})$ and **b** $\text{Li} + \text{Al}(\text{VI})$ vs. $\text{Fe} + \text{Mg} + \text{Mn}$ for the micas belonging to the biotite-zinnwaldite and muscovite-zinnwaldite-polyliithionite trends; **c** $\text{Si} + \text{Li}$ vs. $\text{Al}(\text{tot})$ and **d** $\text{Si} + \text{Li}$ vs. $\text{Fe} + \text{Mg} + \text{Mn} + \text{Al}(\text{IV})$ for the micas belonging to the muscovite-lepidolite trends (all data in a.p.f.u.). The arrows labelled

main exchange vector operating in this case was most probably that of biotite-zinnwaldite ($\text{LiAl}^{\text{VI}}\text{R}_{-2}^{2+}$), with an important decrease in the Mg content parallel to an increase in Li and F (Fig. 7a, b).

6.3 Mineral chemistry of feldspars

All the feldspars associated with the different units of the Tres Arroyos system are alkaline (Table 3, Supplementary Tables 4, 5, Fig. 8). The composition of K-feldspar is in the range of $\text{Or}_{86.75}\text{Or}_{98.08}$, whereas, as expected, plagioclase

with exchange vectors represent the direction of the vector, which indicates the evolutionary trend of the micas. The dashed one corresponds to the biotite-zinnwaldite trend, whereas the continuous line indicates the muscovite-zinnwaldite-polyliithionite and muscovite-lepidolite trends

is richer in Ca in the monzogranite ($\text{Ab}_{75.6}\text{Ab}_{96.4}$) than in the aplopegmatite bodies, which are more fractionated ($\text{Ab}_{96.9}\text{Ab}_{99.9}$).

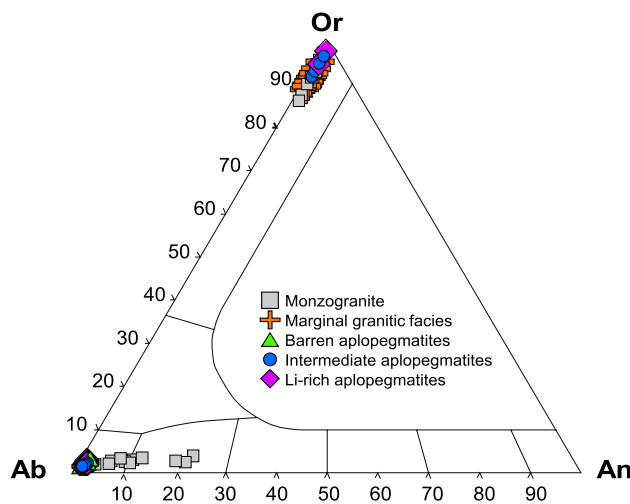
The P contents in the feldspars from the Tres Arroyos system are some of the highest reported to date in pegmatites, with values of up to 2.5 wt% P_2O_5 (London et al. 1999). The contents obtained in the present study are not as high, but values over 1.20 wt% P_2O_5 are still common. These values in K-feldspar increase from 0.16 to 0.86 in the monzogranite to 0.67–1.68 in the marginal granite and 0.86–1.63 in the barren aplopegmatites and then decrease again to 0.1–1.21

Table 3 Representative microprobe and LA-ICP-MS analyses of feldspars from the different facies of the Tres Arroyos aplopegmatite-granite system (oxides given in wt%; cations in a.p.f.u., and trace elements in ppm)

| Lithology | Monzogranite | | | Marginal granitic facies | | | Barren aplopegmatites | | | Intermediate aplopegmatites | | | Li-rich aplopegmatites | |
|---|--------------|--------|--------|--------------------------|--------|--------|-----------------------|--------|--------|-----------------------------|--------|--------|------------------------|--|
| Mineral | Kfs | Kfs | Pl | Kfs | Pl | Kfs | Kfs | Pl | Kfs | Kfs | Pl | Kfs | Pl | |
| SiO ₂ | 64.37 | 64.56 | 65.46 | 63.22 | 68.66 | 63.13 | 64.36 | 68.58 | 63.71 | 63.32 | 67.15 | 63.89 | 68.14 | |
| TiO ₂ | 0.01 | 0.01 | 0.00 | 0.03 | 0.00 | 0.00 | 0.00 | 0.00 | 0.02 | 0.00 | 0.02 | 0.03 | 0.01 | |
| Al ₂ O ₃ | 18.72 | 18.26 | 20.84 | 18.90 | 19.31 | 18.75 | 18.60 | 19.22 | 18.72 | 17.88 | 19.98 | 18.15 | 19.49 | |
| FeO | 0.01 | 0.01 | 0.06 | 0.01 | 0.05 | 0.00 | 0.03 | 0.02 | 0.04 | 0.00 | 0.00 | 0.02 | 0.03 | |
| MnO | 0.01 | 0.02 | 0.00 | 0.00 | 0.01 | 0.00 | 0.00 | 0.02 | 0.00 | 0.00 | 0.00 | 0.00 | 0.00 | |
| MgO | 0.00 | 0.00 | 0.00 | 0.00 | 0.00 | 0.01 | 0.00 | 0.00 | 0.00 | 0.01 | 0.01 | 0.02 | 0.00 | |
| CaO | 0.05 | 0.00 | 2.48 | 0.00 | 0.00 | 0.00 | 0.02 | 0.00 | 0.00 | 0.02 | 0.13 | 0.00 | 0.20 | |
| Na ₂ O | 0.68 | 1.29 | 10.39 | 0.63 | 11.95 | 1.08 | 1.07 | 11.98 | 0.48 | 0.25 | 11.76 | 0.99 | 11.49 | |
| K ₂ O | 15.78 | 14.86 | 0.44 | 15.67 | 0.08 | 15.33 | 14.89 | 0.05 | 15.35 | 15.55 | 0.16 | 14.46 | 0.13 | |
| P ₂ O ₅ | 0.21 | 0.55 | 0.21 | 1.42 | 0.04 | 1.33 | 0.84 | 0.00 | 1.00 | 0.65 | 0.59 | 0.67 | 0.69 | |
| BaO | 0.02 | 0.00 | n.a. | 0.05 | n.a. | 0.01 | 0.00 | n.a. | 0.00 | 0.02 | 0.00 | 0.02 | n.a. | |
| Rb ₂ O | 0.00 | 0.00 | n.a. | 0.00 | n.a. | 0.23 | 0.33 | n.a. | 1.34 | 1.52 | 0.00 | 1.27 | n.a. | |
| Cs ₂ O | 0.00 | 0.01 | n.a. | 0.01 | n.a. | 0.02 | 0.04 | n.a. | 0.01 | 0.06 | 0.00 | 0.01 | n.a. | |
| F | 0.05 | 0.00 | n.a. | 0.00 | n.a. | 0.00 | 0.00 | n.a. | 0.02 | 0.00 | 0.00 | 0.01 | n.a. | |
| Total | 99.92 | 99.56 | 99.88 | 99.94 | 100.09 | 99.89 | 100.18 | 99.88 | 100.70 | 99.28 | 99.79 | 99.53 | 100.19 | |
| O=F | 0.02 | 0.00 | 0.00 | 0.00 | 0.00 | 0.00 | 0.00 | 0.00 | 0.01 | 0.00 | 0.00 | 0.01 | 0.00 | |
| Total | 99.90 | 99.56 | 99.88 | 99.94 | 100.09 | 99.89 | 100.18 | 99.88 | 100.69 | 99.28 | 99.79 | 99.53 | 100.19 | |
| Structural formula on the basis of 32 O atoms | | | | | | | | | | | | | | |
| Si | 11.888 | 11.919 | 11.556 | 11.658 | 11.992 | 11.667 | 11.829 | 12.004 | 11.747 | 11.888 | 11.772 | 11.880 | 11.871 | |
| Ti | 0.001 | 0.001 | 0.000 | 0.004 | 0.000 | 0.000 | 0.000 | 0.000 | 0.003 | 0.000 | 0.002 | 0.004 | 0.002 | |
| Al | 4.075 | 3.973 | 4.337 | 4.108 | 3.974 | 4.083 | 4.030 | 3.965 | 4.069 | 3.955 | 4.128 | 3.977 | 4.001 | |
| Fe ²⁺ | 0.002 | 0.002 | 0.008 | 0.001 | 0.008 | 0.000 | 0.004 | 0.003 | 0.007 | 0.000 | 0.000 | 0.003 | 0.004 | |
| Mn ²⁺ | 0.001 | 0.003 | 0.001 | 0.000 | 0.002 | 0.001 | 0.000 | 0.003 | 0.000 | 0.000 | 0.000 | 0.000 | 0.000 | |
| Mg | 0.001 | 0.000 | 0.001 | 0.000 | 0.000 | 0.002 | 0.000 | 0.004 | 0.001 | 0.003 | 0.000 | 0.005 | 0.004 | |
| Ca | 0.011 | 0.000 | 0.470 | 0.000 | 0.000 | 0.000 | 0.005 | 0.000 | 0.000 | 0.005 | 0.024 | 0.000 | 0.038 | |
| Na | 0.244 | 0.462 | 3.556 | 0.224 | 4.045 | 0.386 | 0.380 | 4.066 | 0.173 | 0.089 | 3.996 | 0.358 | 3.879 | |
| K | 3.717 | 3.500 | 0.099 | 3.686 | 0.017 | 3.614 | 3.490 | 0.011 | 3.610 | 3.723 | 0.035 | 3.429 | 0.030 | |
| P | 0.033 | 0.085 | 0.031 | 0.222 | 0.005 | 0.208 | 0.131 | 0.000 | 0.156 | 0.104 | 0.087 | 0.106 | 0.102 | |
| Ba | 0.002 | 0.000 | 0.000 | 0.004 | 0.000 | 0.001 | 0.000 | 0.000 | 0.000 | 0.001 | 0.000 | 0.001 | 0.000 | |
| Rb | 0.000 | 0.000 | 0.000 | 0.000 | 0.000 | 0.027 | 0.039 | 0.000 | 0.159 | 0.183 | 0.000 | 0.152 | 0.000 | |
| Cs | 0.000 | 0.001 | 0.000 | 0.001 | 0.000 | 0.002 | 0.003 | 0.000 | 0.001 | 0.005 | 0.000 | 0.001 | 0.000 | |
| F | 0.029 | 0.000 | 0.000 | 0.000 | 0.000 | 0.000 | 0.000 | 0.000 | 0.011 | 0.002 | 0.000 | 0.008 | 0.000 | |
| or | 93.557 | 88.331 | 2.395 | 94.175 | 0.412 | 90.322 | 90.079 | 0.274 | 95.427 | 97.499 | 0.863 | 90.525 | 0.753 | |
| ab | 6.135 | 11.669 | 86.217 | 5.731 | 99.588 | 9.653 | 9.797 | 99.724 | 4.573 | 2.342 | 98.555 | 9.443 | 98.282 | |
| an | 0.270 | 0.000 | 11.388 | 0.000 | 0.000 | 0.000 | 0.123 | 0.002 | 0.000 | 0.129 | 0.582 | 0.000 | 0.965 | |
| cel | 0.038 | 0.000 | 0.000 | 0.095 | 0.000 | 0.025 | 0.000 | 0.000 | 0.000 | 0.030 | 0.000 | 0.032 | 0.000 | |
| LA-ICP-MS analyses (ppm) | | | | | | | | | | | | | | |
| Li | 7 | 15 | 3 | 9 | n.a. | 26 | 8 | n.a. | 21 | 20 | 12 | 27 | n.a. | |
| Be | n.a. | n.a. | 2 | 1 | n.a. | n.a. | 3 | 5 | 3 | 4 | 7 | 2 | n.a. | |
| Ni | 0.740 | n.a. | 0.550 | n.a. | n.a. | n.a. | n.a. | n.a. | n.a. | n.a. | n.a. | n.a. | n.a. | |
| Rb | 281 | 590 | 6 | 3320 | n.a. | 5800 | 6490 | 1 | 12540 | 11190 | 3 | 11780 | 12 | |
| Y | n.a. | n.a. | 0.840 | n.a. | n.a. | n.a. | n.a. | n.a. | n.a. | n.a. | n.a. | n.a. | n.a. | |
| Zr | 31 | 0.021 | 12 | 0.156 | n.a. | 1.000 | n.a. | 0.384 | 0.151 | n.a. | n.a. | n.a. | n.a. | |
| Nb | n.a. | n.a. | 0 | n.a. | n.a. | n.a. | n.a. | n.a. | n.a. | n.a. | n.a. | n.a. | n.a. | |
| Sn | n.a. | 9 | 8 | n.a. | n.a. | 52 | 37 | 4 | 15 | 15 | 12 | 30 | 8 | |
| Cs | 2 | 3 | 0.325 | 54 | n.a. | 58 | 278 | 0.174 | 165 | 512 | – | 163 | n.a. | |
| Ba | 148 | 52 | 132 | n.a. | n.a. | n.a. | n.a. | 0.940 | n.a. | n.a. | 1 | n.a. | n.a. | |

Table 3 (continued)

| Lithology | Monzogranite | | | Marginal granitic facies | | Barren aplopegmatites | | Intermediate aplopegmatites | | | Li-rich aplopegmatites | | |
|-----------|--------------|------|-------|--------------------------|------|-----------------------|------|-----------------------------|------|------|------------------------|------|-------|
| Mineral | Kfs | Kfs | Pl | Kfs | Pl | Kfs | Kfs | Pl | Kfs | Kfs | Pl | Kfs | Pl |
| La | 2 | 0 | 10 | n.a. | n.a. | n.a. | n.a. | 0 | n.a. | n.a. | 0 | n.a. | n.a. |
| Ce | 3 | 0 | 18 | n.a. | n.a. | n.a. | n.a. | 0 | n.a. | n.a. | 0 | n.a. | n.a. |
| Pr | 0 | n.a. | 2 | n.a. | n.a. | n.a. | n.a. | n.a. | n.a. | n.a. | n.a. | n.a. | n.a. |
| Nd | n.a. | n.a. | 5 | n.a. | n.a. | n.a. | n.a. | n.a. | n.a. | n.a. | n.a. | n.a. | n.a. |
| Sm | n.a. | n.a. | 1 | n.a. | n.a. | n.a. | n.a. | n.a. | n.a. | n.a. | n.a. | n.a. | n.a. |
| Eu | 0 | 0 | 2 | n.a. | n.a. | n.a. | n.a. | n.a. | n.a. | n.a. | n.a. | n.a. | n.a. |
| Gd | n.a. | n.a. | 0 | n.a. | n.a. | n.a. | n.a. | n.a. | n.a. | n.a. | n.a. | n.a. | n.a. |
| Tb | n.a. | n.a. | 0 | n.a. | n.a. | n.a. | n.a. | n.a. | n.a. | n.a. | n.a. | n.a. | n.a. |
| Dy | n.a. | n.a. | 0 | n.a. | n.a. | n.a. | n.a. | n.a. | n.a. | n.a. | n.a. | n.a. | n.a. |
| Ho | n.a. | n.a. | 0.025 | n.a. | n.a. | n.a. | n.a. | n.a. | n.a. | n.a. | n.a. | n.a. | n.a. |
| Em | n.a. | n.a. | 0.060 | n.a. | n.a. | n.a. | n.a. | n.a. | n.a. | n.a. | n.a. | n.a. | n.a. |
| Tm | n.a. | n.a. | 0.008 | n.a. | n.a. | n.a. | n.a. | n.a. | n.a. | n.a. | n.a. | n.a. | n.a. |
| Yb | n.a. | n.a. | 0.049 | n.a. | n.a. | n.a. | n.a. | n.a. | n.a. | n.a. | n.a. | n.a. | n.a. |
| Lu | n.a. | n.a. | 0.007 | n.a. | n.a. | n.a. | n.a. | n.a. | n.a. | n.a. | n.a. | n.a. | n.a. |
| Ta | 0.055 | n.a. | — | n.a. | n.a. | n.a. | n.a. | n.a. | n.a. | n.a. | — | n.a. | n.a. |
| Tl | 1 | 2 | 0.032 | 11 | n.a. | 22 | 22 | 0.015 | 47 | 50 | 0.019 | 50 | 0.037 |
| Pb | 34 | 37 | 26 | 5 | n.a. | 7 | 3 | 2 | 7 | 8 | 11 | 3 | 2 |

**Fig. 8** Classification of feldspars in the triangle proposed by Phillips and Griffen (1981) (according to the K, Na, and Ca % contents of the analysed samples)

in the intermediate dykes and to 0.66–0.84 in the Li-rich aplopegmatites (all values in wt% P₂O₅) (Table 3, Supplementary Table 4). The plagioclase shows also noticeable changes in the P contents depending on the lithology. The lowest values are found in the granitic facies (0.14–0.54 and 0.04–0.32 wt% P₂O₅ for the monzogranite and the marginal granite, respectively). Again, the highest contents are associated with the barren aplopegmatites (0.50–1.41 wt% P₂O₅), while intermediate but also some high P values are shown by

the plagioclase from the intermediate and Li-rich aplopegmatites (0.29–1.25 and 0.48–0.84 wt% P₂O₅, respectively) (Table 3, Supplementary Table 4). In plagioclase, as well as in K-feldspar, the good negative correlation between Si and (Al + P) suggests that P was incorporated into the feldspar structure through the berlinitic-type substitution AlPSi₂ (Fig. 9). The distribution of P between coexisting K-feldspar and plagioclase is sensitive to fractionation processes involved in pegmatic evolution, and knowledge of it may help to understand the crystallization conditions in pegmatic environments (e.g. London et al. 1999). D_P^{Kfs/Ab} values for the different facies, calculated by dividing the P₂O₅ content of K-feldspar by that of coexisting plagioclase, may be seen in Table 4. Most of them are in the range of 1–1.76, that is, very close to 1.2, the value calculated by London et al. (1999) for K-feldspar and plagioclase pairs crystallized in equilibrium. These values suggest that plagioclase from the granitic and aplopegmatic units of Tres Arroyos crystallized under magmatic conditions. A significantly higher value has only been observed in the marginal granite (15.06). This value corresponds to one of the albitization patches that may be observed inside a K-feldspar crystal in these bodies, suggesting low P contents in the last metasomatic fluids.

The gradual P-increase from the monzogranite to the barren aplopegmatites may be related to the perphosphorous character of the NA batholith. In such melts, the low activity of Ca would prevent apatite crystallization, and P would behave as an incompatible element, thus partitioning

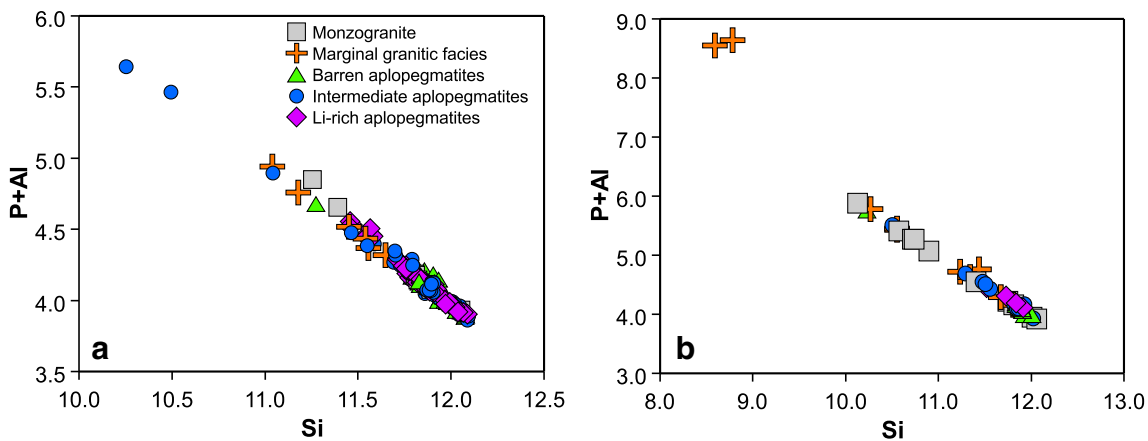


Fig. 9 Plots of Si vs. P+Al for **a** plagioclase and **b** K-feldspar (all data in a.p.f.u.)

Table 4 Calculated P partition coefficients between coexisting K-feldspar and plagioclase in the different facies of the Tres Arroyos aplopegmatite-granite system

| Monzo-granite | Marginal granite | Barren aplopegmatites | Intermediate aplopegmatites | Li-rich aplopegmatites |
|----------------|------------------|-----------------------|-----------------------------|------------------------|
| $D_P^{Kfs/Pl}$ | 1.6 | 15.06 | 0.89 | 1.76 |
| 1 | 3.29 | 2.4 | 1.09 | 1.48 |
| | | 1.62 | 2.16 | |
| | | 1.81 | 1.9 | |
| | | 1.48 | | |

into the residual melt (Bea et al. 1992; London et al. 1999). During the crystallization of these residual melts, P could enter the feldspar lattice, as in the case of the marginal granite and the barren aplopegmatites, as well as the Fe–Mn phosphates, which constitute a common accessory mineral (<3%) that is homogeneously distributed in these bodies. With a higher fractionation degree, feldspars from the intermediate aplopegmatites show a lower P-content, whereas P concentrations in the bulk rock are higher than in the barren aplopegmatites (London et al. 1999; Roda-Robles et al. 2018). This could be the result of the early crystallization of members of the amblygonite-montebrasite series in these dykes, hence lowering the P budget of the melt prior to the feldspars' crystallization, as proposed by London et al. (1999).

Trace element contents in K-feldspar also show important differences in relation to the associated lithology. There are important and continuous increase in the Rb and Cs contents from the monzogranite to the Li-rich aplopegmatites, parallel to the decrease in the Ba contents (131–12400 ppm Rb, 2–512 ppm Cs, 1389–1 ppm Ba) (Fig. 6b, Supplementary Table 5). Some of the Ba contents showed by the feldspars

from the intermediate aplopegmatites are higher than those of the feldspars from the barren dykes and the marginal granitic facies. This is probably related to the lack of Fe-rich micas in the former. Barium partitions preferentially into biotite (or zinnwaldite). When these micas are absent, feldspar becomes the main sink for Ba, hence showing higher values than in those lithologies where Fe-micas are common. Representative chondrite-normalized (McDonough and Sun 1995) REE patterns for the K-feldspar from the two granitic and three aplopegmatitic units from Tres Arroyos are presented in Fig. 10a. The total normalized REE budget (ΣREE_N) for K-feldspar is in the ranges of 2.62–30.89, 0.2–43.76, and 0–0.11 for the monzogranite, marginal granite, and aplopegmatites. The REE patterns for K-feldspar from aplopegmatites are rather incomplete, because the concentrations of most of the HREEs are typically below the LOD (Fig. 10a). Nevertheless, the patterns indicate a slight enrichment in LREEs and depletion towards the HREEs. The total normalized REE budget (ΣREE_N) for plagioclase is also very low (11.03–125.18 and 0–0.27 for the monzogranite and aplopegmatites, respectively) (Fig. 10b). Actually, it was only possible to obtain partial REE analyses of the plagioclase from most of the aplopegmatites, reflecting the extremely low anorthite content ($Ab_{98}–Ab_{100}$), whereas plagioclase associated with the monzogranite shows a pattern similar to that of K-feldspar, with a pronounced positive Eu-anomaly. The magnitude of the Eu-anomaly in K-feldspar decreases with fractionation, and some K-feldspar samples from the marginal granite even show a small negative Eu-anomaly (Fig. 10a). The progressive decrease of the positive Eu-anomaly toward a slightly negative one with fractionation has been previously observed in other zoned pegmatites and pegmatitic fields (e.g., Kontak and Martin 1997; Larsen 2002; Hulsbosch et al. 2014; Michallik et al. 2017) and explained as the result of fractionation of accessory minerals such as monazite. In the case of Tres Arroyos, monazite is

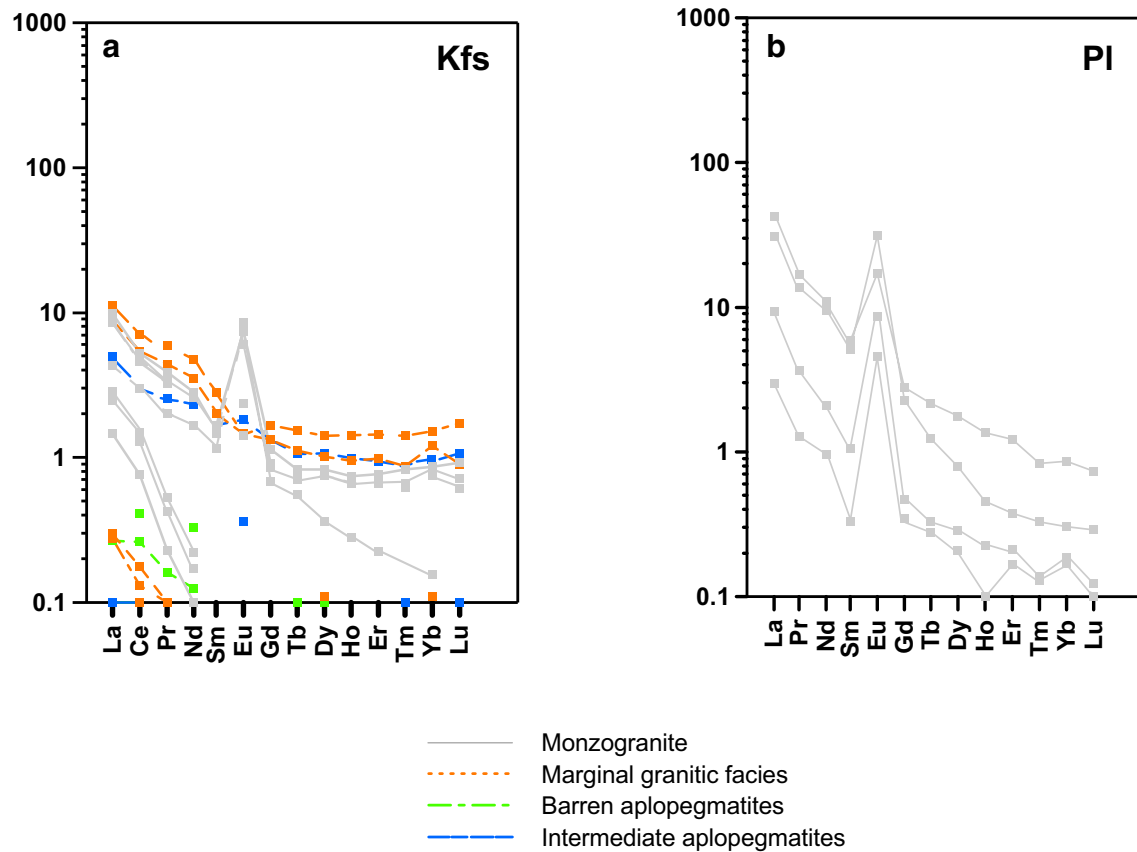


Fig. 10 Representative chondrite-normalized (McDonough and Sun 1995) REE patterns for **a** K-feldspar and **b** plagioclase

only present in the monzogranite, not in the aplopegmatites. Therefore, the REE fractionation should be mostly complete from the beginning of pegmatite crystallization.

6.4 Structural characteristics of micas and K-feldspar

Polytype of the micas from the different aplopegmatite types has been determined by X-ray diffraction techniques (Supplementary Fig. 1). In the barren aplopegmatites $2M_1$ is a common polytype, corresponding to muscovite, whereas IM has been identified in the F-Li-Fe-bearing micas associated with these dykes. Muscovite from the intermediate aplopegmatites shows the $2M_1$ polytype. Finally, in the lithium rich dykes IM is the main polytype found in the case of lepidolite, whereas in the mixed forms, corresponding to intermediate compositions between muscovite and lepidolite, the polytypes $2M_1$ and IM appear in different proportions, interlayered in the same sample (Supplementary Fig. 1).

The studied K-feldspar samples show differences in the structural state, from orthoclase to low microcline, with intermediate order degrees (intermediate microcline) for some of the analysed samples, with $t1(o)-t1(m)$ ranging from

0.00 to 0.90 (Fig. 11a). The degree of order varies depending on the lithology in the Tres Arroyos system. Orthoclase is found in the marginal granite and in nearly all the samples from the three types of aplopegmatites. In contrast, maximum and intermediate microcline are characteristic of most of the K-feldspar crystals analysed from the monzogranite, and one sample from the barren aplopegmatites (Table 5, Fig. 11b). Because the metastable persistence of orthoclase in plutonic rocks may be well explained by the strain retardation of inversion (Eggerton and Buseck 1980), the preservation of monoclinic K-feldspar could be due to: (1) low activity of fluids and/or tectonic stress (Brown and Parsons 1989, 1994), (2) high cooling rate and/or decompression, and (3) presence of large cations in the lattice, such as Rb and Cs (Gordiyenko 1971; Shmakin 1979). Based on the high Rb contents in K-feldspar from most of the aplopegmatites in Tres Arroyos (Table 3, Supplementary Table 4, 5), and their emplacement into colder metasediments with strong loss of fluids, it is conceivable that the two latter factors may have contributed to prevent the inversion. In contrast, K-feldspar crystals from the granite show a higher order degree. In this case, besides the slow cooling rate, the subsolidus activity of fluids, as evidenced by the coarsening of the vein perthites

Fig. 11 Plots of **a** $(t_{1o} - t_{1m})$ vs. $(t_{1o} + t_{1m})$ and **b** $2\theta(240)$ vs. $2\theta(060)$ to characterize the structural state of the studied feldspars (*MM* maximum microcline, *OR* orthoclase, *HS* high sanidine, *LA* low albite, *HA* high albite); and **c** bc vs. a unit cell dimensions for the studied feldspars (“normal” alkaline feldspars plot over the line corresponding to the zero deformation degree, whereas deformed samples plot out from this curve. The distance between the points and the line is a measurement of strain; Bernotat 1982; Kroll and Ribbe 1987). (Cross-contoured in the plots are from Kroll and Ribbe 1983)

to patch perthites, probably favoured the inversion from the monoclinic to the triclinic structure. In this regard, the plot of the a parameter versus $b \times c$ (Fig. 11c) reflects a slight strain for some of the samples, mainly the intermediate microcline from the monzogranite and the orthoclase from the aplopegmatites. “Normal” alkaline feldspars plot over the line corresponding to the zero deformation degree, whereas deformed samples plot out from this curve. Distance between the points and the line is a measurement of strain (Bernotat 1982; Kroll and Ribbe 1987). Deformation presented by the intermediate microcline crystals indicates that the energy released during the inversion from monoclinic orthoclase to triclinic microcline has been lower than the accumulated elastic deformation, and hence, the order in those microcline crystals is not complete (Kroll and Ribbe 1987). The strained orthoclase crystals could present sub-microscopic domains of triclinic symmetry, where Si-Al ordering has already started, as described in Bambauer et al. (1989).

6.5 Behaviour of trace elements during crystallization

Studies on the distribution of trace elements between coexisting silicates during the crystallization of granite-pegmatite systems are relatively rare (see Černý et al. 1985 for an overview; Oyarzábal et al. 2009; Roda-Robles et al. 2012; Merino et al. 2013; Pesquera et al. 2017). Feldspars and micas are the main mineral phases and coexist in all the units of Tres Arroyos. Lithium, Rb, Cs, Ba, Nb, and Ta show a clear tendency to get into the structure of the Fe-rich mica, whereas Be partitions preferably into the Al-micas (Fig. 12). When Fe-micas are absent (i.e., in barren, intermediate, and Li-rich aplopegmatites), Al-micas become the main sink for Li, Rb, Cs, Sn, Nb, and Ta. The only trace elements that get preferentially into the feldspar structure are P and Pb. Feldspars from the five units show relatively high P concentrations, especially for the marginal granite and barren pegmatites. Mean values are higher for K-feldspar than for plagioclase (Fig. 12). In the case of Pb, the main values are quite similar for plagioclase and K-feldspar, with the highest values found in the monzogranite, followed by the intermediate pegmatites, where Al-micas show also relatively high Pb-contents (Fig. 12). The REE contents are in

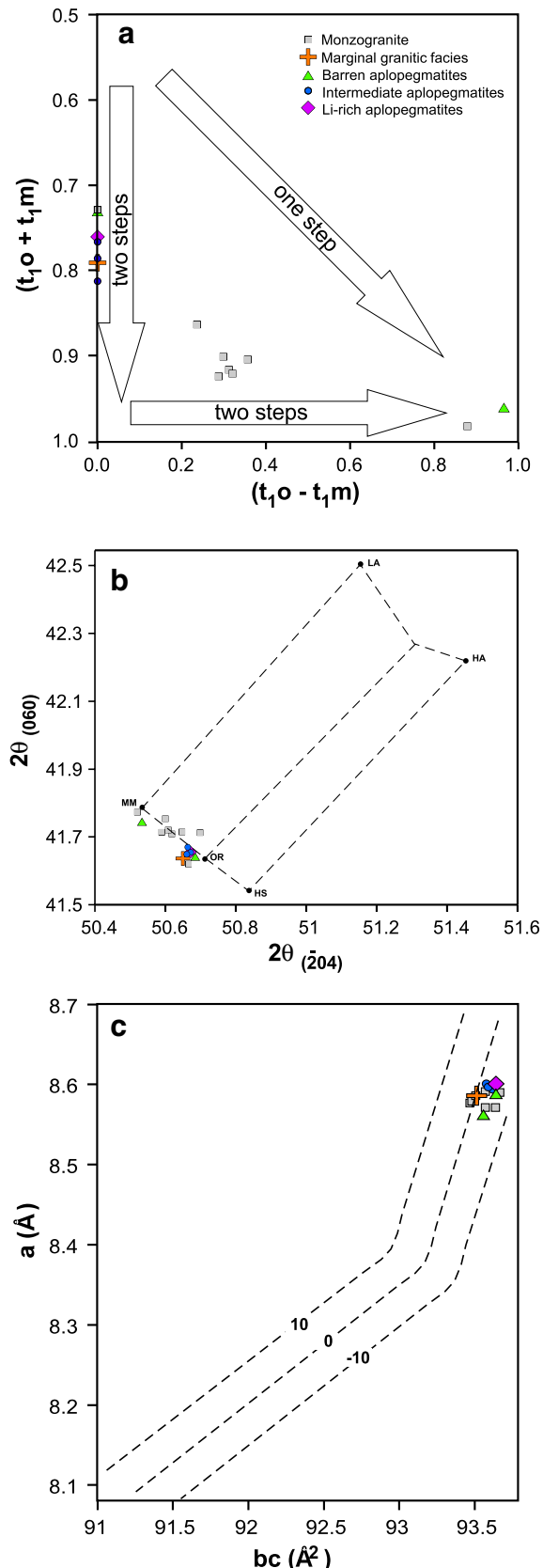


Table 5 a , b , and c unit cell and reciprocal parameters, cell volume and triclinicity values for the studied feldspars (a , b , and c values are in Å; a^* , b^* , and c^* are in Å $^{-1}$; volume is in Å 3 , and the angles are in grades)

| Lithology | a (σ) | b (σ) | c (σ) | α (σ) | β (σ) | γ (σ) | V (σ) | a^* (σ) | b^* (σ) | c^* (σ) | α^* (σ) | β^* (σ) | γ^* (σ) | Δ |
|----------------------------|-----------|-------------|-----------|--------------|--------------|--------------|--------------|---------------|---------------|---------------|----------------|---------------|----------------|------|
| Monzogranite | 8.583 (3) | 12.970 (5) | 7.209 (2) | 90.240 (37) | 115.985 (23) | 89.301 (52) | 721.237 (32) | 0.129626 (51) | 0.077109 (27) | 0.154324 (39) | 90.074 (29) | 64.016 (23) | 90.661 (47) | 0.20 |
| Monzogranite | 8.591 (4) | 12.969 (6) | 7.215 (3) | 90.197 (50) | 116.022 (29) | 89.246 (56) | 722.321 (42) | 0.129539 (61) | 0.077112 (35) | 0.154244 (50) | 90.150 (47) | 63.978 (29) | 90.744 (53) | 0.26 |
| Monzogranite | 8.571 (4) | 12.969 (3) | 7.220 (2) | 90.577 (35) | 115.906 (26) | 87.951 (44) | 721.415 (37) | 0.129791 (46) | 0.077155 (20) | 0.153983 (26) | 90.354 (29) | 64.098 (26) | 91.998 (39) | 0.84 |
| Monzogranite | 8.571 (5) | 12.973 (7) | 7.213 (3) | 90.206 (64) | 115.943 (33) | 89.325 (84) | 721.145 (48) | 0.129751 (64) | 0.077090 (41) | 0.154179 (53) | 90.099 (46) | 64.058 (34) | 90.650 (72) | 0.32 |
| Monzogranite | 8.577 (3) | 12.967 (7) | 7.208 (3) | 90.311 (66) | 115.954 (29) | 89.274 (82) | 720.746 (42) | 0.129680 (47) | 0.077125 (41) | 0.154295 (49) | 90.007 (54) | 64.048 (29) | 90.656 (73) | 0.15 |
| Monzogranite | 8.579 (5) | 12.973 (7) | 7.206 (3) | 90.336 (57) | 115.886 (35) | 89.168 (94) | 721.397 (52) | 0.129581 (93) | 0.077090 (39) | 0.154257 (49) | 90.031 (42) | 64.116 (35) | 90.762 (86) | 0.12 |
| Monzogranite | 8.586 (3) | 12.978 (4) | 7.205 (2) | 90.243 (31) | 115.965 (28) | 89.449 (45) | 721.752 (31) | 0.129555 (43) | 0.077060 (24) | 0.154369 (36) | 89.997 (30) | 64.036 (28) | 90.494 (44) | 0.13 |
| Barren | 8.561 (5) | 12.972 (10) | 7.212 (4) | 90.760 (59) | 115.828 (40) | 87.754 (54) | 720.352 (53) | 0.129866 (81) | 0.077152 (62) | 0.154038 (61) | 90.243 (56) | 64.181 (39) | 87.872 (50) | 0.80 |
| aplopegma- | | | | | | | | | | | | | | |
| Monzogranite | 8.590 (3) | 13.007 (3) | 7.201 (2) | 90.00 | 116.034 (24) | 90.00 | 722.937 (24) | 0.129563 (32) | 0.076884 (18) | 0.154342 (30) | 90.00 | 63.966 (20) | 90.00 | 0 |
| Marginal granitic facies | 8.586 (4) | 12.988 (4) | 7.200 (2) | 90.00 | 116.011 (28) | 90.00 | 721.588 (37) | 0.129595 (64) | 0.076997 (26) | 0.154536 (45) | 90.00 | 63.989 (28) | 90.00 | 0 |
| Barren | 8.587 (2) | 13.005 (2) | 7.200 (1) | 90.00 | 116.013 (13) | 90.00 | 722.615 (19) | 0.129583 (32) | 0.076891 (14) | 0.154345 (23) | 90.00 | 63.987 (13) | 90.00 | 0 |
| aplopegma- | | | | | | | | | | | | | | |
| Intermediate | 8.601 (3) | 12.986 (3) | 7.206 (2) | 90.00 | 116.031 (29) | 90.00 | 723.217 (29) | 0.129389 (47) | 0.077006 (15) | 0.154443 (28) | 90.00 | 63.969 (23) | 90.00 | 0 |
| Intermediate aplopegmatite | 8.594 (2) | 12.997 (2) | 7.203 (1) | 90.00 | 116.027 (18) | 90.00 | 722.932 (18) | 0.129497 (30) | 0.076940 (14) | 0.154502 (23) | 90.00 | 63.973 (17) | 90.00 | 0 |
| Intermediate aplopegmatite | 8.597 (2) | 12.991 (3) | 7.204 (2) | 90.00 | 116.044 (23) | 90.00 | 722.848 (23) | 0.129474 (38) | 0.076975 (15) | 0.154499 (33) | 90.00 | 63.956 (23) | 90.00 | 0 |
| Lithium rich aplopegmatite | 8.601 (2) | 12.998 (3) | 7.204 (1) | 90.00 | 116.051 (19) | 90.00 | 723.598 (19) | 0.129408 (27) | 0.076932 (17) | 0.154511 (25) | 90.00 | 63.949 (15) | 90.00 | 0 |

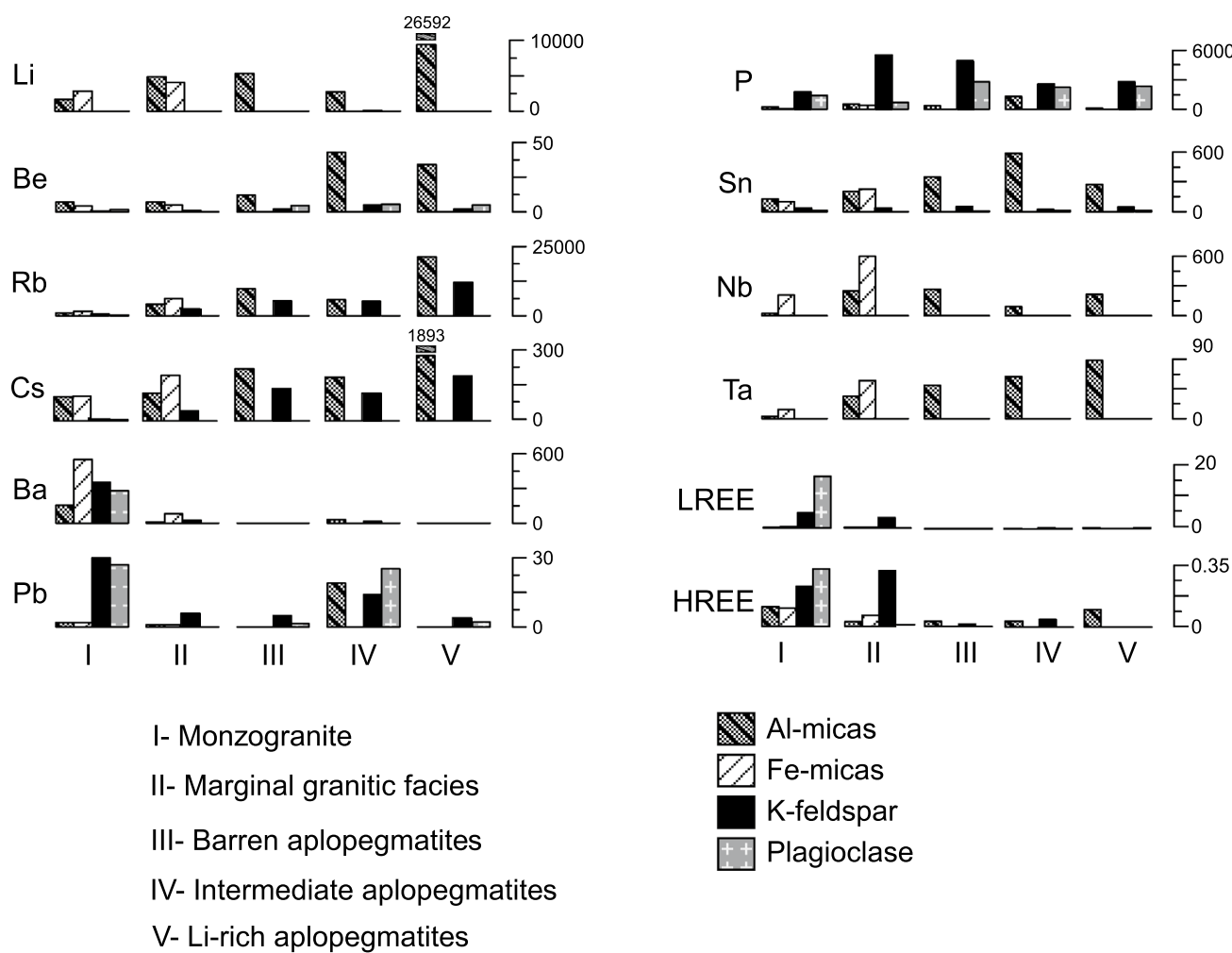


Fig. 12 Trace elements distribution among Al-micas, Fe-micas, K-feldspar, and plagioclase for the different facies from Tres Arroyos (all mean values are in ppm)

general very low for all the minerals from the aplopegmatites (Fig. 12). Comparison between the different mineral phases is only possible in the granitic facies. In the case of the monzogranite, plagioclase is the richest in HREE and LREE contents (Fig. 12). In the case of the marginal granite, where the plagioclase composition corresponds to nearly pure albite, K-feldspar becomes the only mineral with measurable amounts of both HREEs and LREEs (Fig. 12).

The origin of the differences in the distribution of trace elements between the different mineral phases is related to the distinct concentration of the elements in the fractionating melt and the variations in the compatibility of these elements between melt and minerals, which depends on the behaviour of major elements, temperature, pressure, or $f\text{O}_2$. The alkali and alkali-earth elements (e.g., Li, Rb, Cs, Na, K, Be, and Ba) play a significant role during the fractionation of pegmatitic melts (London 2008; Simmons and Webber 2008; Oyarzábal et al. 2009; Roda-Robles et al. 2012; Vieira et al.

2011). In the Tres Arroyos granite-aplopegmatite system, the Li enters preferentially into micas, as in other Li–F-rich pegmatites from the CIZ (Roda-Robles et al. 2012). Rubidium also tends to accumulate in the last melts of pegmatitic systems, although it is more compatible than Li or Cs (London 2005). It easily substitutes for K in the structure of micas and K-feldspar (Trueman and Cerny 1982). Due to its large size and low field strength, Cs is very incompatible in most of the silicates (London et al. 1998; Watson 1976). Mica structure is the most suitable to accommodate Cs, followed by K-feldspar. Beryllium is moderately to strongly compatible in muscovite (London 2005), which is reflected in the high Be-contents of Al-micas in comparison to the other mineral phases in Tres Arroyos (Fig. 12). There is a general decrease in the Ba content from the monzogranite to the Li-rich aplopegmatites for micas and feldspars. It partitions preferentially into the Fe-mica in the two granitic facies, but once Fe-micas are absent, Ba is distributed more or less

equally among Al-mica and K-feldspar. Barium distribution coefficients show a broad spectrum, with positive values for biotite, muscovite, and K-feldspar and negative ones for plagioclase (London 2008). These important variations could be correlated with changes in the temperature, pressure, or composition (Icenhower and London 1996).

The high field strength elements Nb, Ta, and Sn also show important differences in micas and feldspars. Due to the difficulty of fitting into the structure of the most common rock-forming minerals, these elements are incompatible during the crystallization of peraluminous melts, such as that of the Tres Arroyos granite-aplopegmatite system. Mineral/melt partition coefficients (K_D) are scarce for these elements (see Linnen and Cuney 2005 for an overview; Raimbault and Burnol 1998; Pesquera et al. 2017). In Tres Arroyos, Nb and Ta show the highest concentrations in micas, preferentially in the Fe-micas when present (granitic units) and in the Al-micas in the three aplopegmatite types. Trends shown by Nb and Ta are different: while the Ta concentration in mica increases gradually from the monzogranite up to the Li-rich aplopegmatites, Nb contents show a more erratic trend, with ups and downs (Fig. 12). Taking into account the low value of $K_D^{\text{Mu}/\text{melt}}$ for Ta (0.42) (Raimbault and Burnol 1998), the relatively high Ta content of Al-micas in the Tres Arroyos aplopegmatites could be explained by the lack of any other mineral phase competing for Ta, such as the Fe-micas, combined with the gradual fractionation, which would allow the progressive enrichment in Ta of the melts. Finally, Sn also enters preferentially into the micas (the highest values are found in the intermediate aplopegmatites), which is consistent with the data given by Antipin et al. (1981) and Kovaleenko et al. (1977, 1988) with $K_D^{\text{Mu}/\text{melt}}$ higher than 1 for Sn.

6.6 Petrogenetic implications

In the Tres Arroyos granite-aplopegmatite system, there is a complete and continuous geochemical transition from granitic to highly evolved pegmatitic facies, which is less frequently observed in other pegmatitic belts worldwide. Five different units have been distinguished, with increasing degree of fractionation: (1) porphyritic monzogranite (main facies of the NA batholith); (2) marginal granitic facies, rimming the monzogranite in the Tres Arroyos area; (3) barren aplopegmatites hosted in metasediments of the SGC, close to the marginal granite; (4) intermediate leucocratic aplopegmatitic dykes, also hosted in metasediments but further from the granite; and (5) highly evolved Li-rich aplopegmatites, which occur furthest from the contact with the marginal granite (Fig. 1, Table 1). Thus, a regional zoning is observed in the Tres Arroyos granite-aplopegmatite system in relation to the NA batholith.

In contrast to other Li-rich aplopegmatite fields in the northern and central parts of the CIZ (e.g., Lalín-Forcarei Roda-Robles et al. 2016, 2018), the Li-aluminosilicates spodumene and petalite are absent in the Li-rich aplopegmatites from Tres Arroyos. This may be a consequence of the high F activity of the pegmatitic melts, evidenced by the common occurrence of topaz as an accessory mineral even in the less fractionated units, such as the barren aplopegmatites. Taking into account the good positive correlation between Li and F in mica (e.g., Tindle and Webb 1990; Tischendorf et al. 1997, 2004, 2007; Roda-Robles et al. 2006; Roda et al. 2007a; Vieira et al. 2011), it is expected that the first main Li-mineral to crystallize is the Li-mica instead of spodumene or petalite, considering the high activity of F in the melt.

It is well known that the K/Rb ratio in micas and K-feldspar is a good index of the degree of evolution of granites and pegmatites (Černý et al. 1981; Roda-Robles et al. 1993, 2012; Černý and Burt 1984; Foord et al. 1995; Marchal et al. 2014; Roda et al. 2007b; London 2008; Vieira et al. 2011). In general, a linear and continuous variation of the K/Rb ratio versus some elements such as Cs or Li supports the link between granites and pegmatites. It also supports that the fractional crystallization is the main process involved in their chemical evolution (London 2008). The K/Rb proportion decreases gradually from the monzogranite (1966–73 for biotites, 377–123 for muscovites, and 1013–138 for K-feldspar) through the marginal granite (41–27 for biotites, 958–36 for muscovite-zinnwaldite, and 358–34 for K-feldspar), the barren aplopegmatites (21–4 in muscovite-zinnwaldite-polylithionite and 51–19 for K-feldspar), and the intermediate aplopegmatites (67–12 for muscovite and \approx 11 for K-feldspar) up to the lithium-rich dykes, where the lowest K/Rb ratios are found (20–4 for mica and \approx 10 for K-feldspar) (Fig. 6). The K/Rb ratio of micas and K-feldspar from the five lithologies of Tres Arroyos has been plotted versus the contents of the incompatible elements Li, Rb, and Cs and the compatible element Ba (Fig. 6). There is a good negative correlation between the K/Rb ratio and the incompatible elements and a positive one with Ba for both minerals. These plots support an origin of the aplopegmatites via fractional crystallization, starting from the monzogranite and following the sequence: marginal granite, barren, intermediate, and Li-rich aplopegmatites. The study of the trace element distributions in quartz as well as the geochemical modelling carried out by using Rayleigh equations for the fractional crystallization supports this model (Garate-Olave et al. 2017). It is also consistent with London et al. (1999) interpretation that “each successive granite facies at Tres Arroyos represents a (mostly) liquid differentiate that has separated from a cognate crystalline fraction”.

As mentioned before, the aplopegmatites from Tres Arroyos do not present internal zoning (nor quartz cores), as systematic textural, chemical, or mineralogical variations

have not been observed inside the dykes. Indeed, the chemical compositions of micas and feldspars remain mostly equal across the aplopegmatitic bodies. This suggests that during the crystallization of these dykes, fractionation of the melts was negligible. Elbaite, a Li-mineral often occurring in Li-bearing pegmatites, is absent in the Li-rich dykes from Tres Arroyos. The strong tourmalinization occurring in the hosting metasediments of the aplopegmatite dykes, where biotite crystals are pseudomorphically replaced by tiny acicular tourmaline crystals, attests to metasomatic processes involving a H₂O-B-rich fluid exsolved from the pegmatitic-melt. Once the melt is injected into the fractures, the important pressure decrease undergone by the system could lead to the exsolution of such fluids (Roda-Robles et al. 2018). This, together with the fast cooling of the pegmatitic melt in contact with the colder country rocks, would lead to an important undercooling of the melt, which could be related to the lack of chemical variation in micas and feldspars across the dykes, the aplastic character of an important volume of the dykes (Fenn 1977; Nabelek et al. 2010), the development of rhythmic banding (Webber et al. 1997, 1999; London 2008; Nabelek et al. 2010), and other directional textures such as feldspar comb-crystals (Simmons and Webber 2008), which are observed frequently in the aplopegmatites from Tres Arroyos.

7 Conclusions

The main conclusions of this work can be summarized as follows:

1. Five different units constitute the Tres Arroyos granite-aplopegmatite system, with a regional zonal distribution and an increasing degree of fractionation from (1) the monzogranite belonging to the Nisa-Albuquerque batholith; to (2) marginal granite; (3) barren aplopegmatites; (4) intermediate aplopegmatites; and (5) Li-rich aplopegmatites.
2. Micas from the five units define three chemical trends, which include one or two series; *biotite-zinnwaldite*, *muscovite-zinnwaldite-polythionite* and *muscovite-lepidolite*. In general, compositional variation is mainly controlled by the following exchange vectors: muscovite-zinnwaldite ($\text{SiLiAl}_{-1}^{\text{IV}}\text{Vac}_{-1}$); zinnwaldite-polylithionite ($\text{SiLiAl}_{-1}^{\text{IV}}\text{Fe}_{-1}^{2+}$); muscovite-polylithionite ($\text{Li}_2\text{SiAl}_{-1}^{\text{IV}}\text{Al}_{-1}^{\text{VI}}\text{Vac}_{-1}$); muscovite-trilithionite ($\text{Li}_3\text{Al}_{-1}^{\text{VI}}\text{Vac}_{-2}$); and, trilithionite-polylithionite ($\text{Si}_2\text{LiAl}_{-1}^{\text{IV}}\text{Al}_{-2}^{\text{VI}}$).
3. A variable structural state of the K-feldspar is found in the studied rocks: microcline is common in the porphyritic monzogranite, whereas orthoclase is characteristic of the aplopegmatites. The preservation of the mono-

clinic structure in the aplopegmatites may be related to the rapid cooling rate and decompression of the crystallizing melts in open fractures and/or to the high Rb content of most of these K-feldspar crystals.

4. Micas, K-feldspar and, in a lesser extent, plagioclase, are good geochemical indicators of the evolution of the Tres Arroyos granite-aplopegmatite system by using trace elements such as Li, Rb, Cs, Nb, Ta, Sn and P.
5. Li, Rb, Cs, Nb and Ta partition into Fe-micas whereas Be and Sn incorporate preferentially into the Al-mica structure. Lead and P partition into the feldspars, with some variations between plagioclase and K-feldspar.
6. The continuous decrease of the K/Rb ratios in micas and K-feldspar, together with the field observations (mainly the gradual increase of the fractionation degree of the aplopegmatite dykes with distance from the NA batholith), is consistent with a parental relationship between the Nisa-Albuquerque batholith and the aplopegmatites from Tres Arroyos, through a fractional crystallization mechanism.

Acknowledgements The authors thank the Associate Editor, Teresa Ubide, and two anonymous reviewers for their careful reviews and comments, which have helped to improve the manuscript. The authors are indebted to the mining company IMERYS, which has always facilitated access to the quarry. This research has been supported financially by the Spanish Ministerio de Economía y Competitividad (Project CGL2012-31356 through ERDF funds). The University of the Basque Country (UPV/EHU) contributed economically through the grant GIU1216 and GIU1501. Idoia Garate-Olave has been financed by Gobierno Vasco/Eusko Jaurlaritza.

References

- Antipin, V. S., Kovalenko, V. I., Kutnetsova, A. I., & Persikova, L. A. (1981). Distribution coefficients for tin and tungsten in ore-bearing acid igneous rocks. *Geochemistry International*, 18(1), 92–106.
- Bambauer, H. U., Krause, C., & Kroll, H. (1989). TEM-investigation of the sanidine microcline transition across metamorphic zones—the K-feldspar varieties. *European Journal of Mineralogy*, 1(1), 47–58.
- Bea, F., Fershtater, G. B., & Corretgé, L. G. (1992). The geochemistry of phosphorus in granite rocks and the effect of aluminium. *Lithos*, 29, 43–56.
- Bernotat, W. H. (1982). Ein neues Maß für die Verzerrung der Kristallgitters in entmischten alkalifeldspaten [Abstract]. *Fortschritte der Mineralogie*, 60(1), 43–45.
- Breiter, K., Ackerman, L., Svojška, M., & Müller, A. (2013). Behavior of trace elements in quartz from plutons of different geochemical signature: A case study from the Bohemian Massif, Czech Republic. *Lithos*, 175–176, 54–67. <https://doi.org/10.1016/j.lithos.2013.04.023>.
- Brown, W. L., & Parsons, I. (1989). Alkali feldspars—ordering rates, phase-transformations and behavior diagrams for igneous rocks. *Mineralogical Magazine*, 53(369), 25–42. <https://doi.org/10.1180/minmag.1989.053.369.03>.

- Brown, W. L., & Parsons, I. (1994). Feldspars in igneous rocks. In I. Parsons (Ed.), *Feldspars and their reactions* (Vol. 421, pp. 449–499), Nato Advanced Science Institutes Series, Series C, Mathematical and Physical Sciences, Springer.
- Černý, P., & Burt, D. M. (1984). Paragenesis, crystallochemical characteristics, and geochemical evolution of micas in granitic pegmatites. In Bailey S.W. Ed., *Micas. Mineralogical Society of America*, Review in Mineralogy, 13, 257–298.
- Černý, P., Chapman, R., Teertstra, D. K., & Novák, M. (2003). Rubidium-and cesium-dominant micas in granitic pegmatites. *American Mineralogist*, 88, 1832–1835.
- Černý, P., London, D., & Novak, M. (2012). Granitic pegmatites as reflections of their sources. *Elements*, 8, 289–294.
- Černý, P., Meintzer, R. E., & Anderson, A. J. (1985). Extreme fractionation in rare-element granitic pegmatites; selected examples of data and mechanisms. *The Canadian Mineralogist*, 23(3), 381–421.
- Černý, P., Paul, B. J., Hawthorne, F. C., & Chapman, R. (1981). A niobian rutile disordered columbite intergrowth from the Huron claim pegmatite. *Southeastern Manitoba. The Canadian Mineralogist*, 19(4), 541–548.
- Drivenes, K., Larsen, R. B., Müller, A., & Sørensen, B. E. (2016). Crystallization and uplift path of late Variscan granites evidenced by quartz chemistry and fluid inclusions: Example from the Land's End granite, SW England. *Lithos*, 252–253, 57–75. <https://doi.org/10.1016/j.lithos.2016.02.011>.
- Eggerton, R. A., & Buseck, P. R. (1980). The orthoclase-microcline inversion: a high-resolution transmission electron-microscope study and strain analysis. *Contributions to Mineralogy and Petrology*, 74(2), 123–133. <https://doi.org/10.1007/bf01131998>.
- Fenn, P. M. (1977). The nucleation and growth of alkali feldspars from hidrous melts. *The Canadian Mineralogist*, 15, 135–161.
- Foord, E. E., Černý, P., Jackson, L. L., Sherman, D. M., & Eby, R. K. (1995). Mineralogical and geochemical evolution of Micas from Miarolitic Pegmatites of the Anorogenic Pikes-Peak Batholith, Colorado. *Mineralogy and Petrology*, 55(1–3), 1–26.
- Foster, M. D. (1960). Interpretation of the composition of Lithium Micas. *Geological Survey Geological Paper*, 354-E, 115–147.
- Gallego Garrido, M. (1992). Las mineralizaciones de Li asociadas a magmatismo ácido en Extremadura y su encuadre en la Zona Centro-Ibérica. PhD, Universidad Complutense de Madrid, Spain.
- Garate-Olave, I., Müller, A., Roda-Robles, E., Gil-Crespo, P. P., & Pesquera, A. (2017). Extreme fractionation in a granite-pegmatite system documented by quartz chemistry: The case study of Tres Arroyos (Central Iberian Zone, Spain). *Lithos*, 286–287, 162–174.
- González Menéndez, L. (1998). *Petrología y geoquímica del Batolito granítico de Nisa-Alburquerque (Alto Alentejo, Portugal, Extremadura, España)*. Granada: Universidad de Granada.
- González-Menéndez, L., Azor, A., Ordóñez, A. R., & Sánchez-Almazo, I. (2010). The metamorphic aureole of the Nisa-Alburquerque batholith (SW Iberia): implications for deep structure and emplacement mode. *International Journal of Earth Sciences*, 100(7), 1533–1550. <https://doi.org/10.1007/s00531-010-0568-4>.
- Gordiyenko, V. V. (1971). Concentration of Li, Rb, and Cs in potash feldspar and muscovite as criteria for assessing the rare metal mineralization in granite pegmatites. *International Geology Review*, 13, 134–142.
- Hawthorne, F. C., & Černý, P. (1982). Selected peraluminous minerals. In Černý, P. (Ed.), *Granitic pegmatites in Science and Industry. Short Course (MAC)*, 8, 163–186.
- Holland, T. J. B., & Redfern, S. A. T. (1997). Unit cell refinement from powder diffraction data; the use of regression diagnostics. *Mineralogical Magazine*, 61(1), 65–77.
- Hulbosch, N., Hertogen, J., Dewaele, S., Andre, L., & Muchez, P. (2014). Alkali metal and rare earth element evolution of rock-forming minerals from the Gatumba area pegmatites (Rwanda): Quantitative assessment of crystal-melt fractionation in the regional zonation of pegmatite groups. *Geochimica et Cosmochimica Acta*, 132, 349–374. <https://doi.org/10.1016/j.gca.2014.02.006>.
- Icenhower, J., & London, D. (1996). Experimental partitioning of Rb, Cs, Sr, and Ba between alkali feldspar and peraluminous melt. *American Mineralogist*, 81, 719–734.
- Jolliff, B. L., Papike, J. J., & Shearer, C. K. (1992). Petrogenetic relationships between pegmatite and granite based on geochemistry of muscovite in pegmatite wall zones, Black Hills, South Dakota, USA. *Geochimica et Cosmochimica Acta*, 56, 1915–1939.
- Kontak, D. J., & Martin, R. F. (1997). Alkali feldspar in the peraluminous South Mountain Batholith, Nova Scotia: Trace-element data. *The Canadian Mineralogist*, 35(4), 959–977.
- Kovalenko, V. I., Antipin, V. S., Konusova, V. V., Smirnova, Y. V., Petrov, L. L., Vladykin, N. V., et al. (1977). Partition coefficients of fluorine, niobium, tantalum, lanthanum, ytterbium, yttrium, tin and tungsten in Ongonite. *Doklady Earth Science*, 233, 203–205.
- Kovalenko, V. I., Hervig, R. L., & Sheridan, M. F. (1988). Ion-microprobe analyses of trace elements in anorthoclase, hedenbergite, aenigmatite, quartz, apatite, and glass in pantellerite: Evidence for high water contents in pantellerite melt. *American Mineralogist*, 73, 1038–1045.
- Kroll, H., & Ribbe, P. H. (1983). Lattice parameters, composition, and Al/Si order in alkali feldspars. *Feldspar Mineralogy, Reviews in Mineralogy*, 2, 57–100.
- Kroll, H., & Ribbe, P. H. (1987). Determining (Al, Si) distribution and strain in alkali feldspars using lattice-parameters and diffraction-peak positions—a review. *American Mineralogist*, 72(5–6), 491–506.
- Larsen, R. B. (2002). The distribution of rare-earth elements in K-feldspar as an indicator of petrogenetic processes in granitic pegmatites: examples from two pegmatite fields in southern Norway. *The Canadian Mineralogist*, 40, 137–151.
- Linnen, R. L., & Cuney, M. (2005). Granite-related rare-element deposits and experimental constraints on Ta–Nb–W–Sn–Zr–Hf mineralization. In R. L. Linnen, & I. M. Samson (Eds.), *Rare-element geochemistry and mineral deposits* (pp. 45–68), Geol. Assoc. Canada Short Course Notes 17.
- London, D. (2005). Granitic pegmatites: an assessment of current concepts and directions for the future. *Lithos*, 80(1–4), 281–303. <https://doi.org/10.1016/j.lithos.2004.02.009>.
- London, D. (2008). Pegmatites. *The Canadian Mineralogist, Special Publication n°*, 10, 347.
- London, D., Morgan, G. B., & Icenhower, J. (1998). Stability and solubility of pollucite in the granite system at 200 MPa H₂O. *The Canadian Mineralogist*, 36, 497–510.
- London, D., Wolf, M. B., Morgan, G. B., & Garrido, M. G. (1999). Experimental silicate-phosphate equilibria in peraluminous granitic magmas, with a case study of the Alburquerque batholith at Tres Arroyos, Badajoz, Spain. *Journal of Petrology*, 40(1), 215–240.
- Marchal, K. L., Simmons, W. B., Falster, A. U., Webber, K. L., & Roda-Robles, E. (2014). Geochemistry, mineralogy, and evolution of Li-Al micas and feldspars from the Mount Mica pegmatite, Maine, USA. *The Canadian Mineralogist*, 52(2), 221–233. <https://doi.org/10.3749/canmin.52.2.221>.
- Martínez Catalán, J. R., Arenas, R., Díaz García, F., Rubio Pascual, F. J., Abati, J., & Marquinez, J. (1996). Variscan exhumation of a subducted paleozoic continental margin: The basal units of the Ordes Complex, Galicia, NW Spain. *Tectonics*, 15(1), 106–121.
- Martínez, F. J., Julivert, M., Sebastián, A., Arboleda, M. L., & Gil-Ibaraguchi, J. I. (1988). Structural and thermal evolution of high-grade areas in the northwestern parts of the Iberian Massif. *American Journal of Science*, 288, 969–996.

- Martínez-Fernández, F. J. (1974). Estudio del área metamórfica y granítica de los Arribes del Duero (Prov. de Salamanca y Zamora). Universidad de Salamanca.
- McDonough, W.F. & Sun, S.S. (1995). The composition of the earth. *Chemical Geology*, 120, 223–253. [https://doi.org/10.1016/0009-2541\(94\)00140-4](https://doi.org/10.1016/0009-2541(94)00140-4).
- Merino, E., Villaseca, C., Orejana, D., & Jeffries, T. (2013). Gahnite, chrysoberyl and beryl co-occurrence as accessory minerals in a highly evolved peraluminous pluton: The Belvís de Monroy leucogranite (Cáceres, Spain). *Lithos*, 179, 137–156. <https://doi.org/10.1016/j.lithos.2013.08.004>.
- Michallik, R. M., Wagner, T., Fusswinkel, T., Heinonen, J. S., & Heikkilä, P. (2017). Chemical evolution and origin of the Luumäki gem beryl pegmatite: Constraints from mineral trace element chemistry and fractionation modeling. *Lithos*, 274–275, 147–168. <https://doi.org/10.1016/j.lithos.2017.01.001>.
- Monier, G., & Robert, J. L. (1986). Evolution of the miscibility gap between muscovite and biotite solid solutions with increasing lithium content: an experimental study in the system $K_2O-Li_2O-MgO-FeO-Al_2O_3-SiO_2-H_2O-HF$ at 600 °C, 2kbar PH_2O : comparison with natural lithium micas. *Mineralogical Magazine*, 50, 641–651.
- Müller, A., Ihlen, P. M., Snook, B., Larsen, R. B., Flem, B., Bingen, B., et al. (2015). The chemistry of quartz in granitic pegmatites of Southern Norway: Petrogenetic and economic implications. *Economic Geology*, 110, 1737–1757.
- Nabelek, P. I., Whittington, A. G., & Sirbescu, M. L. C. (2010). The role of H_2O in rapid emplacement and crystallization of granite pegmatites: Resolving the paradox of large crystals in highly undercooled melts. *Contributions to Mineralogy and Petrology*, 160(3), 313–325. <https://doi.org/10.1007/s00410-009-0479-1>.
- Noronha, F., Ramos, J. M. F., Rebelo, J., Ribeiro, A., & Ribeiro, M. L. (1981). Essai de corrélations des phases de déformation hercyniennes dans le nord-ouest Péninsulaire. *Leidse Geologische Mededelingen*, 52(1), 87–91.
- Oyarzábal, J., Galliski, M. Á., & Perino, E. (2009). Geochemistry of K-feldspar and Muscovite in Rare-element Pegmatites and Granites from the Totoral Pegmatite Field, San Luis, Argentina. *Resource Geology*, 59(4), 315–329.
- Paton, C., Hellstrom, J., Paul, B., Woodhead, J., & Hergt, J. (2011). Iolite: Freeware for the visualisation and processing of mass spectrometric data. *Journal of Analytical Atomic Spectrometry*, 26(12), 2508. <https://doi.org/10.1039/c1ja10172b>.
- Pekov, I. V., Kononkova, N. N., Agakhanov, A. A., Belakovskiy, D. I., Kazantsev, S. S., & Zubkova, N. V. (2010). Voloshinite, a new rubidium mica from granitic pegmatite of Voron'i Tundras, Kola Peninsula, Russia. *Geology of Ore Deposits*, 52(7), 591–598. <https://doi.org/10.1134/s1075701510070081>.
- Pesquera, A., Gil-Crespo, P. P., Torres-Ruiz, J., & Roda-Robles, E. (2017). Insights into petrogenesis of the Jáalam pluton (Central Iberian Zone, western Spain). *International Geology Review*, 60(2), 157–187.
- Phillips, W. R., & Griffen, D. T. (1981). Optical mineralogy: Nonopaque Minerals. San Francisco.
- Pouchou, J. L., & Pichoir, F. (1985). “PAP” $\varphi(\rho Z)$ procedure for improved quantitative microanalysis. In J. T. Armstrong (Ed.), Microbeam analysis (pp. 104–106): San Francisco Press.
- Raimbault, I., & Burnol, L. (1998). The Richemont rhyolitic dyke, Massif Central, France: a subvolcanic equivalent of rare-metal granites. *The Canadian Mineralogist*, 36, 265–282.
- Roda, E., Keller, P., Pesquera, A., & Fontan, F. (2007a). Micas of the muscovite–lepidolite series from Karibib pegmatites, Namibia. *Mineralogical Magazine*, 71(1), 41–62. <https://doi.org/10.1180/minmag.2007.071.1.41>.
- Roda, E., Pesquera, A., Velasco, F., & Fontan, F. (1999). The granitic pegmatites of the Fregeneda area (Salamanca, Spain): characteristics and petrogenesis. *Mineralogical Magazine*, 63(4), 535–558.
- Roda, E., Vieira, R., Lima, A., Pesquera, A., Noronha, F., & Fontan, F. (2007b). The Fregeneda—Almendra pegmatitic field (Spain & Portugal): mineral assemblages and regional zonation. *Granitic Pegmatites: The State of the Art—International Symposium*(May), 3–4.
- Roda-Robles, E., Pesquera, A., Gil-Crespo, P., & Torres-Ruiz, J. (2012). From granite to highly evolved pegmatite: A case study of the Pinilla de Fermoselle granite–pegmatite system (Zamora, Spain). *Lithos*, 153, 192–207. <https://doi.org/10.1016/j.lithos.2012.04.027>.
- Roda-Robles, E., Pesquera, A., Gil-Crespo, P. P., Torres-Ruiz, J., & De Parseval, P. (2006). Mineralogy and geochemistry of micas from the Pinilla de Fermoselle pegmatite (Zamora, Spain). *European Journal of Mineralogy*, 18(3), 369–377.
- Roda-Robles, E., Pesquera, A., Gil-Crespo, P. P., Vieira, R., Lima, A., Garate-Olave, I., et al. (2016). Geology and mineralogy of Li mineralization in the Central Iberian Zone (Spain and Portugal). *Mineralogical Magazine*, 80(1), 103–126. <https://doi.org/10.1180/minmag.2016.080.049>.
- Roda-Robles, E., Pesquera, A., & Velasco, F. (1993). Mica and K-feldspar as indicators of pegmatite evolution the Fregeneda area (Salamanca, Spain). In Fenoll Hach-Alf P., T.-R. J., and F. Gervill (Eds) Current research in geology applied to ore deposits (pp. 653–656). Granada.
- Roda-Robles, E., Simmons, W., Pesquera, A., Gil-Crespo, P. P., Nizamoff, J., & Torres-Ruiz, J. (2015). Tourmaline as a petrogenetic monitor of the origin and evolution of the Berry-Havey pegmatite (Maine, USA). *American Mineralogist*, 100(1), 95–109. <https://doi.org/10.2138/am-2015-4829>.
- Roda-Robles, E., Villaseca, C., Pesquera, A., Gil-Crespo, P. P., Vieira, R., Lima, A., et al. (2018). Petrogenetic relationships among Variscan granitoids and Li-(F-P)-rich aplite-pegmatotes in Central Iberian Zone: geological and geochemical constraints and implications for the other regions from the European Variscides. *Ore Geology Reviews*, 95, 408–430. <https://doi.org/10.1016/j.oregeorev.2018.02.027>.
- Santos-García, J.A. and Casas-Ruiz, J. (1978) Mapa geológico y Memoria de la Hoja 727 (Albuquerque). Mapa Geológico de España E. 1:50.000 ITGE, 33.
- Shmakin, B. M. (1979). Composition and structural state of K-feldspar from U.S. pegmatites. *American Mineralogist*, 64, 49–56.
- Simmons, W. B. S., & Webber, K. L. (2008). Pegmatite genesis: state of the art. *European Journal of Mineralogy*, 20(4), 421–438. <https://doi.org/10.1127/0935-1221/2008/0020-1833>.
- Smith, J.V. (1974). Feldspar minerals. Vol. II: Chemical and textural properties. Springer, 690.
- Solá, A. R., Ribeiro, M. L., Moreira, M. E., & Moreira, M. (1998). Complexo eruptivo de Nisacartografia geoquímica e mecanismo de implantação. Paper presented at the Actas do V Congresso Nacional de Geologia, Lisboa. Comunicações do Instituto Geológico e Mineiro Lisboa.
- Solá, A. R., Williams, I. S., Neiva, A. M. R., & Ribeiro, M. L. (2009). U-Th–Pb SHRIMP ages and oxygen isotope composition of zircon from two contrasting late Variscan granitoids, Nisa-Albuquerque batholith, SW Iberian Massif: Petrologic and regional implications. *Lithos*, 111(3–4), 156–167. <https://doi.org/10.1016/j.lithos.2009.03.045>.
- Tindle, A. G., & Webb, P. C. (1990). Estimation of lithium contents in trioctahedral micas using microprobe data: application to micas from granitic rocks. *European Journal of Mineralogy*, 5, 595–610.
- Tischendorf, G., Förster, H. J., Gottesmann, B., & Rieder, M. (2007). True and brittle micas: composition and solid-solution series. *Mineralogical Magazine*, 71(3), 285–320.

- Tischendorf, G., Gottesmann, B., Foerster, H.-J., & Trumbull, R. B. (1997). On Li-bearing micas; estimating Li from electron microprobe analyses and an improved diagram for graphical representation. *Mineralogical Magazine*, 61(6), 809–834.
- Tischendorf, G., Rieder, M., Forster, H. J., Gottesmann, B., & Guidotti, C. V. (2004). A new graphical presentation and subdivision of potassium micas. *Mineralogical Magazine*, 68(4), 649–667.
- Trueman, D. L., & Cerny. (1982). Exploration for rare-element granitic pegmatites. In: Short course in granitic pegmatites in science and industry. Mineralogical Association of Canada Short Course Handbook, 8, 463–493.
- Vieira, R., Roda-Robles, E., Pesquera, A., & Lima, A. (2011). Chemical variation and significance of micas from the Fregeneda-Almendra pegmatitic field (Central-Iberian Zone, Spain and Portugal). *American Mineralogist*, 96(4), 637–645. <https://doi.org/10.2138/am.2011.3584>.
- Watson, E. B. (1976). Two-liquid partition coefficients: Experimental data and geochemical implications. *Contributions to Mineralogy and Petrology*, 56, 119–134.
- Webber, K. L., Falster, A. U., Simmons, W. B., & Foord, E. E. (1997). The role of diffusion-controlled oscillatory nucleation in the formation of line rock in pegmatite-aplite dikes. *Journal of Petrology*, 38(12), 1777–1791.
- Webber, K. L., Simmons, W. B., Falster, A. U., & Foord, E. E. (1999). Cooling rates and crystallization dynamics of shallow level pegmatite-aplite dikes, San Diego County, California. *American Mineralogist*, 84(5–6), 708–717.
- Whitney, D.L. & Evans, B.W. (2010). Abbreviations for names of rock-forming minerals. *American Mineralogist*, 95, 185–187. <https://doi.org/10.2138/am.2010.3371>
- Wise, M. A., & Brown, C. D. (2010). Mineral chemistry, petrology and geochemistry of the Sebago granite-pegmatite system, Southern Maine, USA. *Journal of Geosciences*, 55(1), 3–26. <https://doi.org/10.3190/jgeosci.061>.

Affiliations

I. Garate-Olave¹ · E. Roda-Robles¹ · P. P. Gil-Crespo¹ · A. Pesquera¹

✉ I. Garate-Olave
idoia.garate@ehu.eu

¹ Dpto. Mineralogía y Petrología, Univ. País Vasco-UPV/EHU, Barrio Sarriena s/n, 48940 Leioa, Spain